

Master's thesis

Marlene Judith Taranger King

Passive Oscillating Foils for Additional Propulsion under Calm Conditions

Master's thesis in Marine Technology

Supervisor: Pål Furset Lader

June 2019

NTNU
Norwegian University of Science and Technology
Faculty of Engineering
Department of Marine Technology

 **NTNU**

Norwegian University of
Science and Technology

Marlene Judith Taranger King

Passive Oscillating Foils for Additional Propulsion under Calm Conditions

Master's thesis in Marine Technology
Supervisor: Pål Furset Lader
June 2019

Norwegian University of Science and Technology
Faculty of Engineering
Department of Marine Technology

 **NTNU**
Norwegian University of
Science and Technology

Summary

This thesis investigates concepts for making the Ocean Cleanup's passive cleanup system, System 001, drift faster under calm conditions. As the system operates in the Great Pacific Garbage Patch (GPGP) in the North Pacific Ocean, the weather in this area was analysed in order to come up with concepts that could utilise the calm conditions more efficiently. Thus, for this thesis, a significant wave height, H_s , of 0.8586 m , a peak wave period, T_p , of 3.9872 s and a wavelength, λ , of 24.8213 m was used to model the wave conditions in the area.

Multiple concepts, such as kites, rudders, and sails were discussed as possible solutions. However, this thesis considers the use of passive oscillating foils for additional propulsion. The foil profile used was a symmetrical NACA 0012 profile in order generate thrust on both the up- and down-stroke, and are placed 12 m below the surface. Further, the foil had a chord length of $c = 1$ m and span $b = 2$ m for the purpose of the calculations in this thesis

The model for this thesis was set up by use of quasi-static theory and the thrust was calculated by use of empirical data. The thrust obtained by the foil was found to be 116 N. However, taking the rest of the system into account, the total increase in velocity was found to be 0.1952 m/s . As the system is assumed to drift at a speed of 0.0735 m/s prior to the installation of foils, the results indicate that the system may be able to increase its speed by 165%. This indicates that under the given conditions, the system will be able to move faster, and thus will potentially also be able to move faster than the plastic by use of passive oscillating foils.

It is however important to keep in mind that the results are based on multiple assumptions and would have to be calculated more carefully before the concept can be applied in real life. This could, for instance, be done by use of CFD (Computational Fluid Dynamics). In addition, it would be relevant to compare this concept to other concepts that utilise waves in order to determine whether this is the best solution. Further, it would also be relevant to compare with concepts that utilise wind and currents.

Sammendrag

Denne masteroppgaven tar for seg ulike konsepter som kan bidra til å øke hastigheten til the Ocean Cleanup sitt pilot prosjekt, System 001. Etersom systemet opererer i Stillehavet, mellom Hawaii og California, var det naturlig å bruke værdata fra dette området til å finne konsepter som kan utnytte rolige sjøtilstander mer effektivt. I denne oppgaven har en signifikant bølgehøyde, H_s , på 0.8586 m , en bølgeperiode, T_p , på 3.9872 s og en bølgelengde, λ , på 24.8213 m blitt brukt for å modellere været i området.

Flere konsepter ble diskutert som mulige løsninger, som blant annet kiter, ror og seil. Denne oppgaven vil i midlertid ta for seg bruken av passivt oscillerende foiler for å øke framdriften til systemet. Foilen som ble brukt i denne modellen er en NACA 0012 symmetrisk foil for å kunne generere framdrift når den beveger seg opp og ned vertikalt, og er plassert 12 m under havoverflaten. Videre har foilen en kordelengde $c = 1\text{ m}$ og et spenn $b = 2\text{ m}$.

Modellen bruker kvasi-statisk teori og beregningene for framdrift er gjort ved bruk av empirisk data. Den totale framdriften generert av foilen ble funnet til å være 116 N . Ved å ta hele systemet inn i betraktning ble den totale økte hastigheten funnet til å være 0.1952 m/s . Etersom systemet var antatt å drifte med en hastighet på 0.0735 m/s uten bruk av passivt oscillerende foiler, indikerer resultatene at hastigheten vil øke med 165% . Resultatene indikerer dermed at under de gitte værtilstandene brukt i denne modellen vil systemet bevege seg raskere, og vil da potensielt også kunne bevege seg raskere enn plastikken.

Det er i midlertid viktig å bemerke seg at disse resultatene er basert på flere antakelser. Det er dermed nødvendig å finregne på dette på et senere tidspunkt, for eksempel ved hjelp av numerisk hydrodynamikk. I tillegg, vil det være relevant å sammenligne dette konseptet med andre konsepter som utnytter bølgene i området. Videre vil det også være relevant å sammenligne dette konseptet med konsepter som tar i bruk andre krefter, som vind og strømning.

Preface

The following thesis *Passive Oscillating Foils for Additional Propulsion under Calm Conditions* is the concluding work of a 5-year Master of Science degree at the Department of Marine Technology at NTNU in Trondheim. This thesis is written as a concept development thesis with a focus on the hydrodynamic feasibility of concepts. The reader will be taken on a path, starting by defining the problem, looking at possible concepts that can contribute to solving the problem, and finally, investigate the feasibility of one of these concepts.

The topic for this project thesis is self-chosen and the work has been done independently with guidance from my supervisor Pål Lader, professor at the Department of Marine Technology, NTNU. I would like to thank my supervisor for being helpful and challenging me along this process. Further, I would like to thank the professors at the Department of Marine Technology (IMT), especially professors specialising in hydrodynamics, for always being available and up for discussion.

In addition, I would like to thank my fellow students of office C1.084 for the support, guidance, and encouragement throughout this semester. I also benefited from discussing issues with my friends and fellow students. I hope you enjoy your reading.

Marlene King
Marlene Judith Taranger King

Trondheim, 07/06/19
Place, date

Contents

| | |
|--|------------|
| Summary | i |
| Sammendrag | ii |
| Preface | iii |
| 1 Introduction | 1 |
| 1.1 Background | 1 |
| 1.2 Objective | 2 |
| 1.2.1 Scope of work | 3 |
| 1.3 Limitations | 3 |
| 1.4 Outline of thesis | 3 |
| 2 The Ocean Cleanup | 5 |
| 2.1 Ocean dynamics | 6 |
| 2.1.1 The gyres | 6 |
| 2.1.2 The North Pacific Gyre | 8 |
| 2.2 Concept description | 9 |
| 2.2.1 System 001 | 11 |
| 2.2.2 Challenges observed | 13 |
| 3 Weather Data | 15 |
| 3.1 Collecting weather data | 15 |
| 3.1.1 Wind data | 16 |
| 3.1.2 Wave data | 18 |
| 3.1.3 Weather data summary | 20 |
| 4 Concept Development | 23 |
| 4.1 Propulsion concepts | 23 |
| 4.2 Foil theory | 28 |
| 4.2.1 Quasi-static theory | 30 |
| 4.3 Potential concepts | 32 |
| 4.3.1 Wave glider | 32 |

| | | |
|----------|--|-----------|
| 4.3.2 | Foils with adjustable flaps | 34 |
| 4.3.3 | Oscillating foils | 35 |
| 5 | Modelling | 39 |
| 5.1 | Wave motions | 39 |
| 5.1.1 | Particle velocity | 39 |
| 5.2 | System movements | 42 |
| 5.2.1 | Relative movement between floater and screen | 42 |
| 5.2.2 | Foil characteristics | 43 |
| 5.3 | Oscillation | 45 |
| 5.3.1 | Pitching | 47 |
| 5.3.2 | Heaving | 49 |
| 5.3.3 | Added mass | 50 |
| 5.3.4 | Spring stiffness | 51 |
| 5.4 | Iteration process | 52 |
| 5.5 | Assumptions | 52 |
| 5.6 | Current force on System 001 | 53 |
| 5.6.1 | Force on floater | 53 |
| 5.6.2 | Forces on screen | 54 |
| 5.6.3 | Total thrust | 55 |
| 6 | Results | 57 |
| 6.1 | Wave characteristics | 57 |
| 6.1.1 | Heave motion, velocity and acceleration | 58 |
| 6.1.2 | Effective inflow velocity, $V(t)$ | 59 |
| 6.2 | Foil characteristics | 60 |
| 6.3 | Forces acting on foil | 60 |
| 6.3.1 | Experimental lift and drag coefficients, C_L and C_D | 61 |
| 6.3.2 | Added mass | 62 |
| 6.4 | State of equilibrium | 62 |
| 6.4.1 | Pivot point, x_p , and spring stiffness, k_s | 63 |
| 6.4.2 | Angles | 65 |
| 6.5 | Calculating thrust | 67 |
| 6.5.1 | Forces on System 001 | 68 |
| 7 | Discussion | 69 |
| 7.1 | Concept choice | 69 |
| 7.2 | Model design | 70 |
| 8 | Conclusion | 71 |
| 9 | Further work | 73 |
| | References | 75 |

| | | |
|-----------------|--|----------|
| Appendix | | I |
| A | MATLAB-script | I |
| A.1 | weather_data.m | I |
| A.2 | foil_thrust.m | III |
| A.3 | spring_pivot_plot.m | VI |
| A.4 | total_thrust.m | VII |
| B | Drag and lift coefficients | XII |
| B.1 | Drag and lift coefficients for NACA 0012 at $R_N = 80,000$ from experiments | XII |

List of Figures

| | | |
|------|---|----|
| 2.1 | Schematic overview of the ocean currents. | 6 |
| 2.2 | Illustration of the Ekman spiral. | 8 |
| 2.3 | Model of the ocean plastic mass concentration for August 2015. . . | 9 |
| 2.4 | Illustration of the forces acting on the system. | 10 |
| 2.5 | The plastic life cycle from it is captured until it is collected. | 10 |
| 2.6 | Front view of the system. | 11 |
| 2.7 | Illustration of loads acting on the system. | 12 |
| 2.8 | Interaction between the currents and the cleanup system. | 13 |
| 2.9 | Configuration after widening the span of the system. | 14 |
| 3.1 | Wind data from 2016 in m/s | 16 |
| 3.2 | Wind data from 2017 in m/s | 17 |
| 3.3 | Wind data from 2018 in m/s | 17 |
| 3.4 | Significant wave height data from 2016 in m | 18 |
| 3.5 | Significant wave height data from 2017 in m | 18 |
| 3.6 | Significant wave height data from 2018 in m | 19 |
| 3.7 | Illustration of a wave with height, wavelength and depth. | 20 |
| 4.1 | Using inflatable buoys as sails to utilise the wind more efficiently. . | 24 |
| 4.2 | Slowing down the system. | 25 |
| 4.3 | Use of rigid foils as sails and rudders. | 26 |
| 4.4 | Attaching foil with rotational springs under the floater. | 27 |
| 4.5 | Utilising foils to close off the U-shape of the system. | 28 |
| 4.6 | 2D foil geometry. | 28 |
| 4.7 | Visualisation of the effect of unsteady flow on a foil. | 29 |
| 4.8 | 2D foil with angle of attack | 30 |
| 4.9 | Angle of attack on a foil. | 31 |
| 4.10 | Vorticity dynamics in drag versus thrust wakes. | 32 |
| 4.11 | Illustration of a wave glider. | 33 |
| 4.12 | Operational mechanism of wave glider. | 33 |
| 4.13 | Foil with different flap sizes. | 35 |
| 4.14 | Schematic illustration of a semi-active flapping foil with forced heave motion. | 36 |

| | | |
|------|--|------|
| 4.15 | Schematic representation of the foil kinematics. | 37 |
| 5.1 | Illustration of the path a particle takes on the surface in waves. . . | 40 |
| 5.2 | Stokes drift particle displacement. | 40 |
| 5.3 | The effect of Stokes drift in the vertical direction. | 41 |
| 5.4 | Water particle orbit in deep water. | 42 |
| 5.5 | Effective inflow velocity on foil. | 44 |
| 5.6 | Definition of angles $\alpha(t)$, $\theta(t)$ and $\phi(t)$ | 44 |
| 5.7 | Angles of attack relative to vertical inflow. | 45 |
| 5.8 | Phase difference between heave, h , and pitch, θ , when $\psi = 90^\circ$ | 46 |
| 5.9 | A foil experiencing stall will no longer produce lift. | 47 |
| 5.10 | Foil pitching in a range of 180° | 47 |
| 5.11 | Phase difference between heave and pitch motion. | 48 |
| 5.12 | Pivot point position. | 49 |
| 5.13 | Analytical added mass coefficient for 3D bodies in infinite fluid. . . | 50 |
| 5.14 | Floater position relative to the surface. | 53 |
| 5.15 | Streamlines passing under the system. | 54 |
| 5.16 | Streamlines past a flat plate. | 55 |
| 6.1 | Reference points A-F during one wave period. | 58 |
| 6.2 | Effective inflow velocity, $V(t)$ | 59 |
| 6.3 | Lift and drag coefficients for a NACA 0012 foil at $R_N = 80,000$. . . | 61 |
| 6.4 | Relationship between pivot point, spring stiffness and thrust produced. | 64 |
| 6.5 | Pitch angles for fixed spring stiffness. | 66 |
| 6.6 | Lift force acting on the foil. | 67 |
| 1 | α , C_L and C_D for a NACA 0012 profile with $R_N = 80,000$ | XII |
| 2 | α , C_L and C_D for a NACA 0012 profile with $R_N = 80,000$ | XIII |

List of Tables

- 3.1 Minimum values for the weather data in the GPGP. 20
- 6.1 Wave characteristics. 58
- 6.2 Heave motion, velocity and acceleration. 58
- 6.3 Foil dimensions. 60
- 6.4 Added mass on hydrofoil. 62

Nomenclature

List of Abbreviations

| | |
|------|------------------------------|
| AoA | Angle of attack |
| CFD | Computational Fluid Dynamics |
| GPGP | Great Pacific Garbage Patch |
| HDPE | High-density polyethylene |
| LE | Leading edge |
| LOA | Length Overall |

List of Symbols

| | |
|---------------------|--|
| α | Angle of attack |
| \ddot{h} | Heave acceleration |
| \dot{h} | Heave velocity |
| λ | Wave length |
| λ_s | Mesh size |
| ν | Kinematic viscosity = $1.18 \cdot 10^{-6}$ for sea water |
| ω | Wave frequency |
| $\bar{T}_{foil,qs}$ | Mean thrust force by use of quasi-static theory |

| | |
|---------------|--|
| ϕ | Inflow angle |
| ψ | Phase angle |
| ρ | Density = $1025\text{kg}/\text{m}^3$ for sea water |
| θ | Pitch angle |
| θ_0 | Initial pitch angle |
| ζ_a | Wave amplitude |
| a | Half of the projected chord length, $c_{proj}/2$ |
| b | Span |
| c | Chord length |
| C_A | Added mass coefficient |
| C_D | Drag coefficient |
| C_L | Lift coefficient |
| C_N | Normal-force coefficient |
| c_w | Phase velocity |
| $C_{L\alpha}$ | Lift coefficient dependent on α |
| C_{Lc} | Lift coefficient dependent on camber |
| c_{proj} | Projected chord length |
| D | Drag force |
| D_s | Twine diameter |
| D_{sys} | Drag force on System 001 |
| F_A | Added mass force |
| F_{ext} | External force |

| | |
|--------------|---------------------------------------|
| F_{hydro} | Hydrodynamic force |
| F_{spring} | Spring force |
| g | Acceleration of gravity = $9.81m/s^2$ |
| h | Heave motion |
| h_0 | Initial foil position |
| H_s | Significant wave height |
| k | Wave number |
| k_s | Spring stiffness |
| L | Lift force |
| l | Depth of screen = $3 m$ |
| m_A | Added mass |
| M_{hydro} | Hydrodynamic moment |
| M_{spring} | Spring moment |
| R_N | Reynolds number |
| S | Area of foil |
| Sn | Solidity |
| T | Thrust force |
| t | Time variable |
| T_p | Peak wave period |
| T_s | Wave period |
| T_{ins} | Instantaneous thrust force |
| U | Net horizontal drift velocity |

| | |
|-----------|--|
| V | Incoming fluid velocity |
| V_R | Reference volume |
| V_{sys} | Total velocity of system |
| w | Vertical particle velocity |
| w_{rel} | Linearised vertical velocity |
| x | Position along the chord |
| x_a | Center of added mass force |
| x_f | Center of lift and drag force |
| x_p | Pivot point |
| x_s | Position along a wave |
| z | Vertical coordinate, z positive upwards, $z = 0$ mean waterlevel |
| z_1 | Mean vertical position of fluid particle |

Chapter 1

Introduction

Oceanic plastic pollution is a widespread problem with heavily documented environmental, ecological and economic impacts (Sherman & van Sebille, 2016). In order to limit the marine plastic problem, the input of plastic to the marine environment must be stopped. Nevertheless, by removing marine plastic that is already in the ocean, the harmful impact can be reduced. The Ocean Cleanup has created a prototype system, named System 001, with the intention of cleaning up the ocean without inflicting harm on the environment. By making use of the winds, currents, and waves in the ocean, the system will drift in the same patterns as the plastic, but at a higher speed. However, during the pilot project, it was observed that under certain conditions, the system was not able to retain the plastic that had been accumulated.

1.1 Background

According to the World Economic Forum (2016), more than 8 million *tonnes* of plastic leak into the ocean every year. This number is expected to increase and by 2050 there will be more plastic than fish in the ocean by mass (Gray, 2018). Plastic is the most common type of marine litter and it is estimated that 80% of the total marine litter is plastic (UNEP, 2014). Once the plastic enters the ocean, it can take hundreds of years before the plastic breaks down into smaller particles, but nevertheless, it is still damaging to the environment (World Economic Forum, 2016). For the wild ecosystems of the ocean, entanglement and ingestion are two of the most harmful impacts of marine litter, leading to injury, illness, suffocation, starvation and death (Gregory, 2009). One of the organisations that are taking action to reduce plastic pollution in the oceans is The Ocean Cleanup. Based in the

Netherlands, CEO Boyan Slat came up with the idea to create a passive cleanup system. The system was launched in August of 2018 when it was transported from San Francisco in California to the "Great Pacific Garbage Patch", a natural accumulation point for marine debris off the west coast of the USA.

As approximately 60% of the plastic produced is less dense than seawater, the Ocean Cleanup has focused on accumulating the plastic drifting on the surface and in the top layers of the ocean. When buoyant plastic enters the ocean, it can be transported by surface currents and winds, degraded into smaller pieces by the sun, temperature variations, waves and also marine life. The plastic can also lose buoyancy and sink to the sea floor where the light does not affect the plastic, resulting in a reduction in the rate of degradation of the plastic (Lebreton et al., 2018). This plastic eventually accumulates in "gyres" characterised as a system of large-scale rotating currents. There are five gyres in the world, with two in the North and South Pacific Ocean, two in the North and South Atlantic Ocean and one in the Indian Ocean. Due to the rotation of the Earth and the wind patterns, these ocean systems are constantly moving. The largest one is found in the North Pacific Ocean and is often referred to as the "Great Pacific Garbage Patch" or GPGP.

Although the Ocean Cleanup's pilot project proved that System 001 was able to collect plastic, the plastic was also observed leaving the system again under certain conditions. In other words, the system was not able to drift at a sufficient speed to retain the plastic accumulated under calm conditions. At the time of writing, the Ocean Cleanup is looking for solutions to the retention problem by making the system drift faster, especially under calm conditions.

1.2 Objective

Due to the retention problem System 001 is experiencing, it became relevant to look at possible solutions to this problem. Thus, the objective of this thesis is related to the development of concepts that address this retention problem. In addition, this thesis will include a feasibility study of the concept of choice in order to determine if the concept investigated is a feasible solution, or a promising avenue of investigation, to the retention problem.

1.2.1 Scope of work

The scope of this thesis is summarised in the following points:

- Conduct a literature review to obtain a better understanding of System 001 and the principles behind the concept. This includes understanding how the natural forces in the area are utilised, as well as gaining a better understanding of the challenges the system is experiencing based on early experience.
- Conduct a weather data analysis for the Great Pacific Garbage Patch (GPGP) by use of Copernicus Climate Data Store. Further, the calm weather conditions in the area can be determined.
- Look into different concepts and ways of utilising the natural forces in the area more efficiently. Choose one concept that will be researched thoroughly and used for the feasibility study.
- Create a model of the concept to use in the feasibility study.
- Simulate the model in MATLAB and determine the feasibility of the concept.
- Conclude with a recommendation of whether the concept of choice can be used for additional propulsion for System 001 under calm conditions or not.

1.3 Limitations

Assumptions had to be made with regards to the system, as there was limited data available. In addition, simplifications regarding the model set-up and simulation in MATLAB had to be made in order to get an estimate of the feasibility. These will be presented as they are taken into use during the course of this thesis.

1.4 Outline of thesis

Chapter 2 describes the ocean dynamics used in the concept of System 001. It also includes the dimensions of the system, as well as the challenges related to the retention of plastic under certain weather conditions.

In Chapter 3 the weather in the area of interest was extracted from Copernicus Climate Data Store and analysed to define the calm weather periods where System 001 is not able to retain the plastic it has accumulated previously.

The concept development phase of the thesis is presented in Chapter 4. This chapter also includes basic theory used to develop the different concepts. In addition, this chapter states which concept is used further for the feasibility study.

Chapter 5 presents how this concept is modelled before determining the feasibility of the concept in Chapter 6.

Chapter 2

The Ocean Cleanup

According to Sherman and van Sebille (2016), both cleanups and source reduction can and must happen in parallel in order to reduce the impact of plastic pollution in our oceans (Rochman, 2016). The Ocean Cleanup has initiated a project to remove plastic debris from the garbage patch in the North Pacific Ocean, also referred to as the Great Pacific Garbage Patch (GPGP). The pilot project is called System 001 and is the world's first ocean cleanup system (The Ocean Cleanup, n.d.-d). The concept is built on the natural ocean dynamics in the area and is an alternative to other solutions that are based on vessels with nets essentially fishing for plastic. It would likely take hundreds of years and billions of dollars to clean up the ocean by using nets towed by vessels. In addition, by-catch and higher emissions would likely be problematic using this approach. Using a passive collection approach, the operational expenses can potentially be very low and the system may be harmless to marine ecosystems as no nets would be used. This makes System 001 to a more viable solution to the cleanup problem (Slat et al., 2014).

The following chapter includes a thorough explanation of the ocean dynamics in the GPGP, the principle of ocean circulations, and how the GPGP ended up being a plastic hotspot. Further, the concept behind the Ocean Cleanup's System 001 will be explained, together with the system characteristics. Finally, the challenges the pilot project has been facing will be discussed.

2.1 Ocean dynamics

All motions of the Earth, including winds and sea currents, are affected by the rotation of the Earth. The wind gives energy to the sea surface and results in currents, while the currents transport heat from one location to another. As a result, the temperature patterns on the surface of the Earth alter and affect the air above. The interaction between the two systems is essential as one system acts to alter the properties of the other system (Sverdrup, 2008).

The large scale circulation of water in the upper layers of the oceans are characterised as wind driven. Wind-driven circulation is considered to be mainly horizontal water transport. The friction between the wind and the ocean surface transfers energy into the surface layer of the ocean and sets the water in this layer in motion. This wind stress is a major cause of the circulation in the upper few hundred meters of the open ocean areas (Yttervik, 2004). Friction between the different layers in the water columns causes the water in the lower layers to start moving too. However, as the deeper layers move more slowly than the upper layers, a spiral, called the Ekman spiral, is formed.

2.1.1 The gyres

The largest circulations of water in the upper layers are often referred to as ocean gyres. There are five major gyres in the world's oceans. These are the North Pacific Gyre (1), the Indian Ocean Gyre (2), the South Pacific Gyre (3), the South Atlantic Gyre (4) and the North Atlantic Gyre (5), respectively. Figure 2.1 below represents these five major gyres.



Figure 2.1: Schematic overview of the five rotating currents where floating plastic accumulates. Often referred to as gyres (ABM Yacht Support, 2017).

A gyre is a vast circular system made up of ocean currents that spiral around a central point. In the Northern Hemisphere these gyres rotate clockwise, while in the Southern Hemisphere, the gyres rotate counter-clockwise (Yttervik, 2004). Once the water is in motion, additional forces come into effect. The most important force is the Coriolis Force, which affects any motion of an object subject to little or no friction, such as wind and surface ocean systems. As the frictional coupling between the ocean water and the Earth's surface is small, the moving water is deflected by the rotation of the Earth (Sverdrup, 2008). A description of the phenomena used to describe the ocean gyres is further described in this chapter.

The Coriolis Effect

The Coriolis Effect is an apparent deflection of a body in motion with respect to a rotating frame of reference (Myrhaug, 2006). However, the body does not actually deviate from its path. It only appears to do so due to the rotating reference frame, which in this case is the Earth (Amdahl et al., 2014). In the Northern Hemisphere, the object is deflected to the right of its origin, while in the Southern Hemisphere it is deflected to the left. The Coriolis Effect is zero at the equator (Slat et al., 2014).

The Ekman Motion

The Ekman Motion is a theory of wind-driven currents not parallel to the wind direction itself (Colling, Brown, & Open University Oceanography Course Team, 2001). It is common to consider the ocean to consist of an infinite number of horizontal layers, where the top layer is subjected to friction by the wind on the top surface, while the lower surface is subjected to friction from the layer below. As the layers are moving in relation to the Earth, all layers are also affected by the Coriolis Force. Thus, the balance between the friction and the Coriolis Force on the infinite number of layers results in an exponential decrease in the speed of the wind-driven current with depth. This is illustrated in Figure 2.2 below.

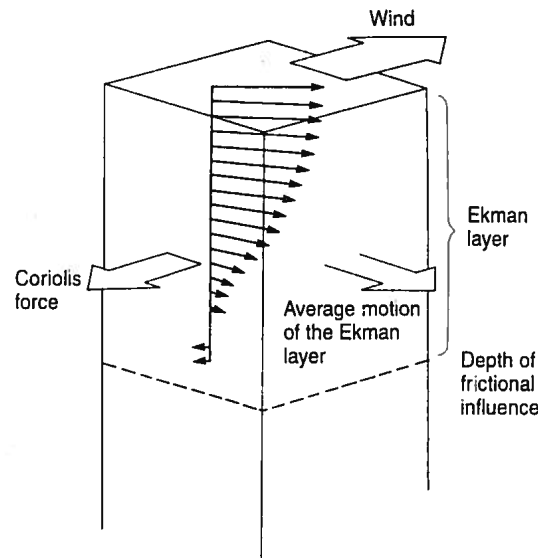


Figure 2.2: Illustration of the Ekman spiral (Bigg, 2003).

The Ekman model predicts that a steady wind blowing across the ocean would cause surface waters to move with an angle of 45° to the right and left of the wind in the Northern and Southern Hemisphere, respectively. Thus, the current vectors form a spiral pattern known as the Ekman spiral. According to this model, the water will have a theoretical net movement throughout the depth of the water column equal to 90° . This is often referred to as the Ekman transport and causes the surface waters to move towards the central region of a gyre (Slat et al., 2014).

2.1.2 The North Pacific Gyre

The North Pacific Gyre is one of the largest oceanic gyres, covering a vast surface area of the ocean. The prevailing wind and current structures in this area are anticyclonic, which results in convergence to the centre of the clockwise rotation (Howell, Bograd, Morishige, Seki, & Polovina, 2012; Colling et al., 2001). The gyre is also often referred to as the Great Pacific Garbage Patch due to a large amount of reported marine debris in this area.

Research conducted in 2015 indicates that the GPGP consists of an area twice the size of France where marine debris has accumulated over many years (Lebreton et al., 2018). Figure 2.3 below illustrates the ocean plastic mass concentration in the GPGP in 2015 and is concentrated in the area between California and Hawaii. As seen in the figure, the concentration is higher closer to the centre of the gyre. This is due to the hydrodynamic processes and the distribution of major plastic

pollution sources (Slat et al., 2014). The GPGP is expected to consist of 1.8 trillion pieces, or 80,000 *tonnes* of plastic. If the outer patch defined by a concentration of 1 kg/km^2 is also considered, the amount of plastic in the GPGP is 100,000 *tonnes*.

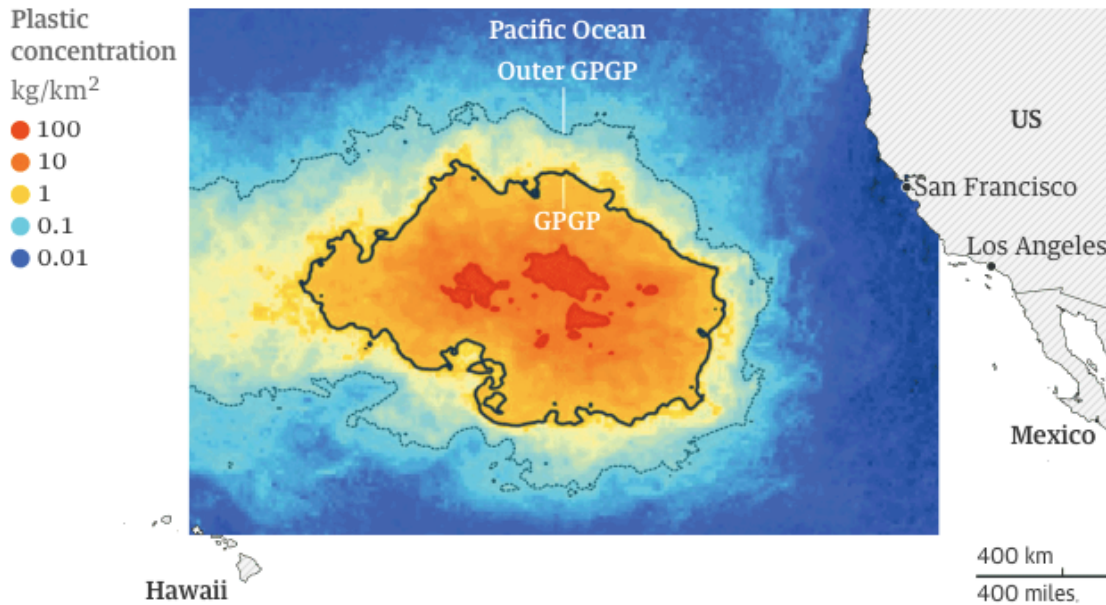


Figure 2.3: Model of the ocean plastic mass concentration for August 2015 (GeoGarage, 2018).

2.2 Concept description

The idea behind System 001 was to create a passive cleanup system by making use of the natural parameters that decide the drifting pattern of the plastic. The Ocean Cleanup has focused on placing plastic collectors in the regions with the largest density of plastic on the surface, such as the GPGP (Sherman & van Sebille, 2016). Thus the Ocean Cleanup decided to launch the pilot project at this location. The goal was to create a concept that will remove a significant amount of ocean plastic as effectively as possible.

Some of the advantages of using a passive collection approach are that it needs less maintenance and the operational expenses can potentially be very low, making this concept more viable. Although the technology is built on simple principles, the dynamics are complex. Wind, waves, and currents act on the plastic and contribute to its drift. However, the main forces contributing to this drift are the wind and currents, where the wind is the dominating force acting on plastic floating on the

surface, while current is the dominant force for submerged microplastic (Bigg, 2003). Figure 2.4 is an illustration of the system seen from above.

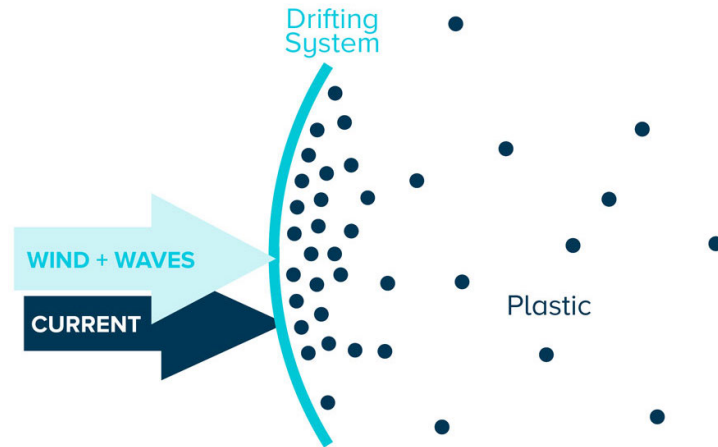


Figure 2.4: Illustration of the forces acting on the system (The Ocean Cleanup, n.d.-a). View from above.

The plastic is captured and accumulated by the U-shaped system floating faster than the plastic. A vessel acting as a garbage truck collects the plastic periodically from the system for reprocessing on land. Figure 2.5 describes this process.

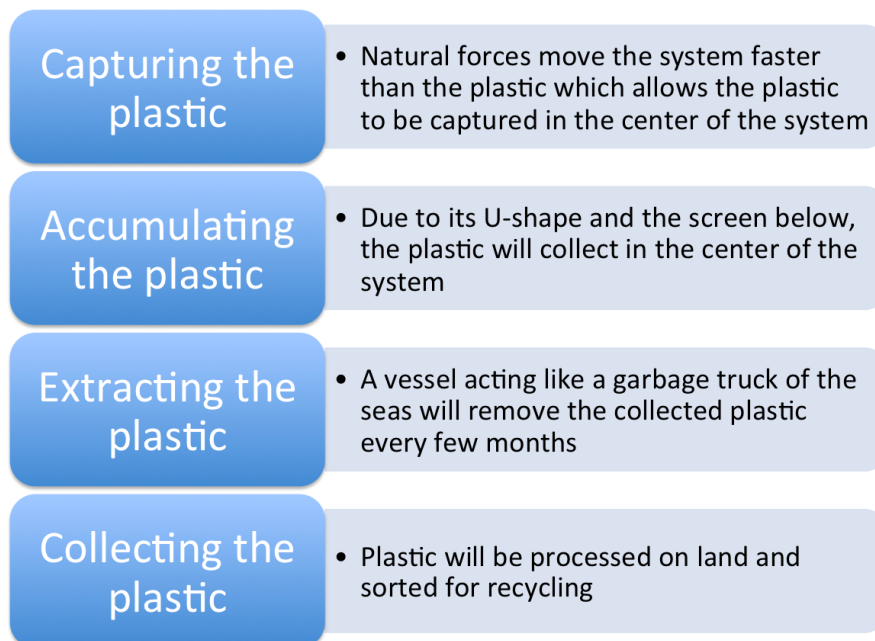


Figure 2.5: The plastic life cycle from it is captured until it is collected.

2.2.1 System 001

In August 2017, The Ocean Cleanup finalised the design of the first ocean cleanup system, after several years of engineering and testing. The pipe structure is designed with a length of 600 *m* and a diameter of 1.2 *m*. In addition, the floater is made out of a stiffer HDPE plastic in order to resist the impact from the ocean under extreme conditions (The Ocean Cleanup, n.d.-c). The pipe is designed so that it is flexible enough to follow the motion of the waves but stiff enough to keep the U-shape used to collect the plastic through the entire operation. The U-shape is retained by is done by using closing lines which are also used to prevent the system from flipping "inside-out" in case the wind turns 180°.

The screen below the pipe is 3 *m* deep and is designed so that the system will be able to collect submerged plastic, both in calm water and in waves where the system does not follow the surface of the water perfectly. Large scale experiments conducted in the GPGP show that with a screen of 2-3 *m*, most of the total plastic mass will be collected. The height of the screen varies along the length in order to reduce the drag of the system. Figure 2.6 below shows the dimensions of the system and how the screen is attached to the floater.

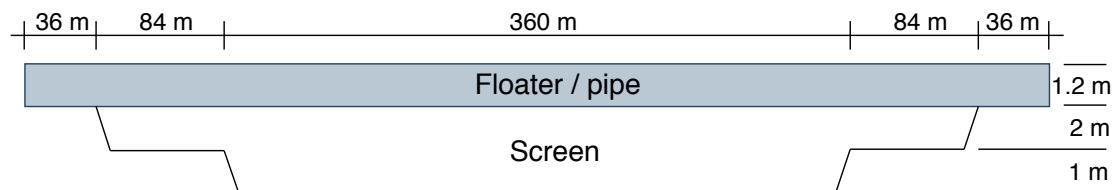


Figure 2.6: Front view of the system.

Solar power

The system will also solely rely on the sun upon providing power to everything from AIS to satellite communication, cameras and sensors. As the system does not have a propulsion system, the location of deployment has to be carefully calculated. Algorithms help specify the optimal deployment location based on expected sea conditions (The Ocean Cleanup, n.d.-b).

Loads on the system

In addition, the screen is impenetrable, which means that wildlife will not be able to get stuck in the screen. The system also travels at a very low speed, which means the marine creatures will be able to swim away from the system (The Ocean Cleanup, n.d.-b). The wind loads will have a direct impact on the part of the system above the water, while the wave loads will impact the system in and under the surface. The plastic is virtually unaffected by the wind and waves, and drifts with the ocean currents (Slat, 2018). Figure 2.7 below illustrates the loads acting on the system.

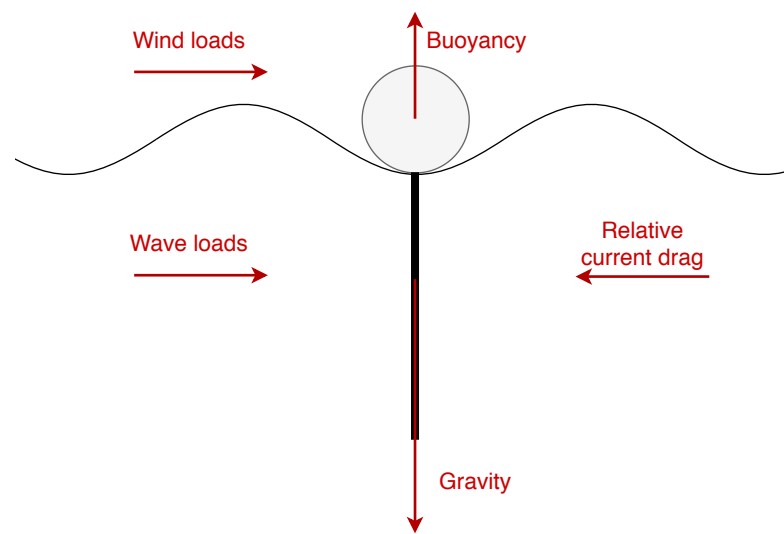


Figure 2.7: Illustration of loads acting on the system.

Expectations and goals

The objective of the system is to accumulate as much plastic in the GPGP as possible, before being extracted by a collecting shuttle vessel acting like a garbage truck at sea. The system is expected to be able to collect plastic ranging from small pieces up to large debris, such as ghost nets, which can be tens of meters wide. If the system works according to the models used to test this concept, it will be able to clean up 50% of the plastic in the GPGP in five years. The Ocean Cleanup also believes that up to 90% of the plastic in the ocean can be removed by 2040 if everything goes according to plan. If System 001 works, the Ocean Cleanup can expand its concept to the other four gyres and clean up oceans all over the world.

2.2.2 Challenges observed

During the first few weeks after deployment of System 001, the system proved that very small pieces of plastic seemed to get caught too. In addition, there were no signs of wildlife interactions. However, the plastic gathered occasionally left the system again. In other words, the system is attracting and concentrating plastic but is not always able to retain it. It was therefore concluded that under certain conditions, the system was not able to drift with a higher speed than the plastic it had collected, as the speed difference between the system and the plastic appeared to be reversed. Thus, the plastic left the system again before the garbage vessel was able to collect the debris.

Some hypotheses to why this is happening include that the force of the wind against the system might be making both extreme ends of the floater pipe oscillate. This leads to a motion force against the wind direction. Another theory is that the vibrations at the ends of the U-shape are creating a type of ripple-force field that repels the plastic away as it nears the mouth of the system. This may be due to the length of the boom and that it is too short.

In addition, stagnation effects have been observed, where small patches of plastic are driven around the system and accumulate on the exterior of the system. Waves also seem to be reflected or radiated at various points, which could affect the ability of the plastic to enter the system (The Ocean Cleanup, 2018a). Figure 2.8 illustrates the interactions between the currents carrying the plastic and the cleanup system, and some of the effects this might have.

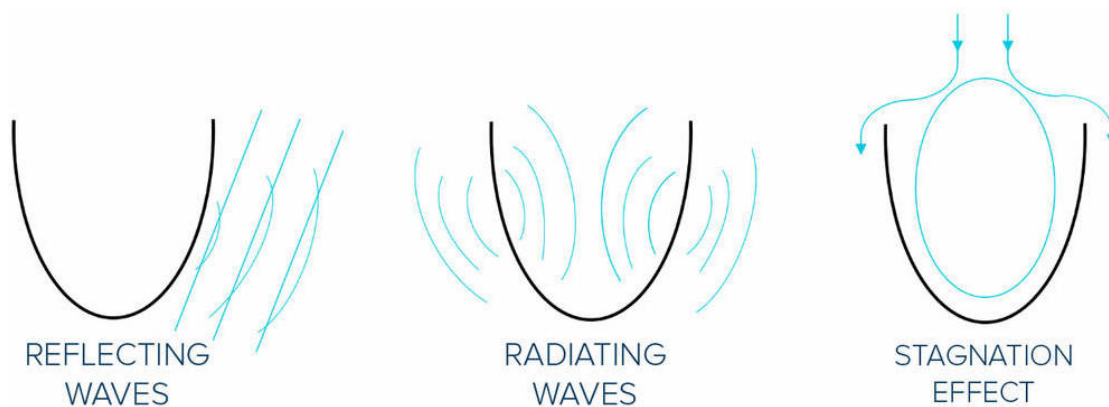


Figure 2.8: Interaction between the currents carrying the plastic and the cleanup system (The Ocean Cleanup, 2018a).

Attempted solution

An attempt to solve the retention problem included widening the span of the system. This was done by changing the closing line configuration of the system and opening the U-shape 60-70 *m* wider. This would result in an increased surface area exposed to wind and waves, potentially increasing the drag acting on the system, and thus also the drifting speed. Figure 2.9 below illustrates the increased wind and wave forces acting on the system by widening the span. However, the Ocean Cleanup has later reported that widening the span of the system did not have the effect they were hoping for (The Ocean Cleanup, 2018a).

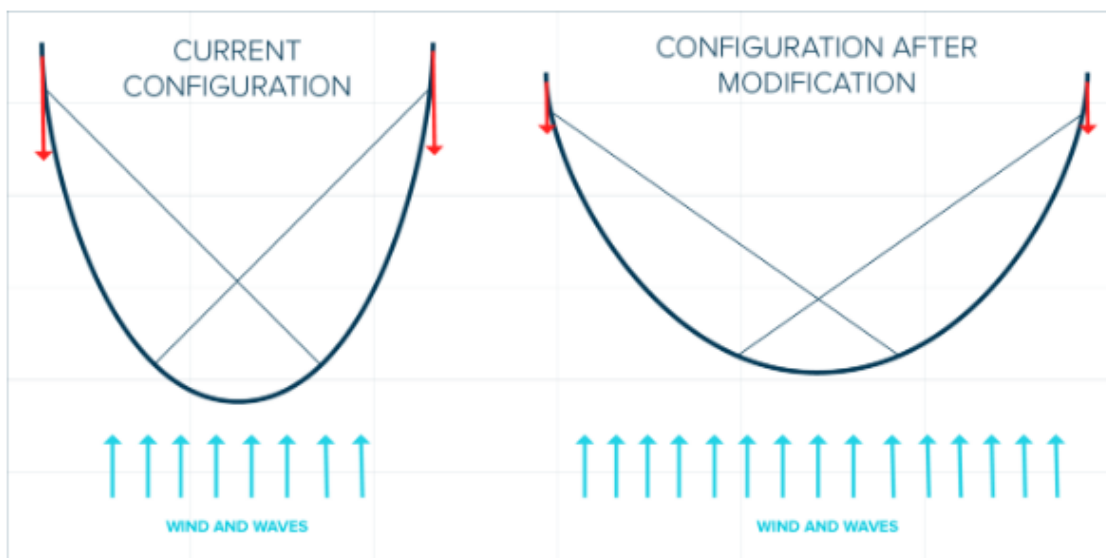


Figure 2.9: Configuration after widening the span of the system.

As the Ocean Cleanup looked at changing the configuration of the system, without success, it was determined that this aspect of the retention problem was too advanced for the purpose of this thesis without having access to additional data about the system.

Further, it is beyond the scope of this thesis to determine the reasons why the system is drifting too slowly. The focus, going forward, will be on concepts that can contribute to additional propulsion without changing the configuration of the system. In order to come up with possible concepts, it was relevant to gain a deeper understanding of the weather conditions in the area.

Chapter 3

Weather Data

As mentioned in Section 2.2.2, one of the main challenges is that the system is not able to retain the plastic under certain weather conditions (The Ocean Cleanup, 2018b). According to the Ocean Cleanup, the main issue is related to the system's ability to drift at a higher speed than the plastic at all times. The objective of this thesis includes looking at possible solutions to increase the speed of the system under these conditions. In order to do so, it is relevant to look into the weather data in the area of interest to understand the environmental conditions.

3.1 Collecting weather data

The first step was to collect data for the area of interest. This was done by using the Copernicus Climate Data Store and downloading the relevant data registered during the period of one year. However, it was also of interest to compare this data with data from previous years to look at the change in weather from one year to the next and also to check that there were no extreme values. Data were therefore collected for the past three years (2016-2018). Information about currents in this area was not available through this portal and it was therefore decided that wind and waves would be the focus going forward.

The Great Pacific Garbage Patch is located roughly between 42° N and 30° N, and 155° W and 135° W (Latitude, 2018). Thus, the weather data for this area was extracted and the parameters collected were as follows:

- 10 m wind speed [m/s]. Referring to the wind speed 10 m above the surface.
- Peak wave period [s].
- Significant height of combined wind waves and swell [m].

3.1.1 Wind data

Wind data from the GPGP was used to determine how the wind speed varies from one day to another. Figure 3.1, 3.2 and 3.3 represent the wind data for the GPGP in 2016, 2017 and 2018, respectively. As seen in the figures, the wind speed varies greatly over the area of interest. The registered wind speed varies from $2 m/s$ to over $26 m/s$ over the course of these three years. As 2018 had a higher average wind speed over the area of interest than the two previous years, the lowest value registered over the past three years was used going forward.

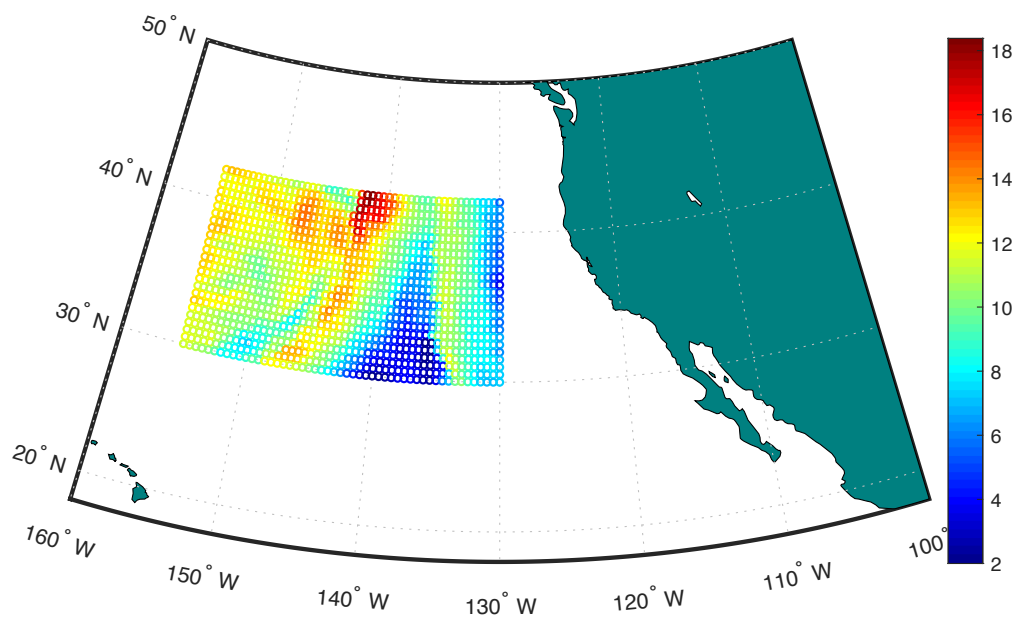
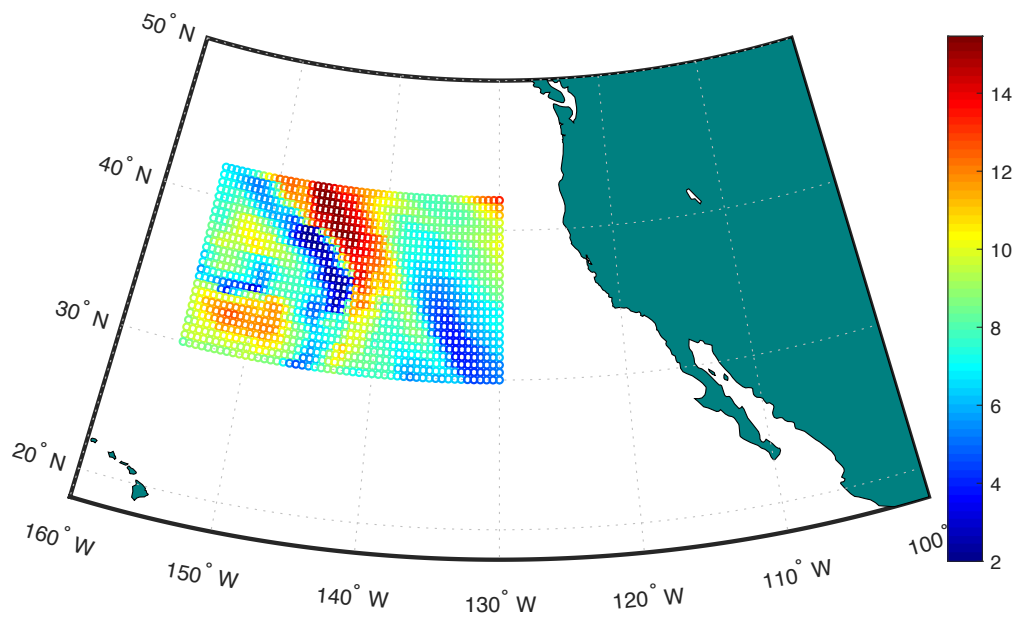
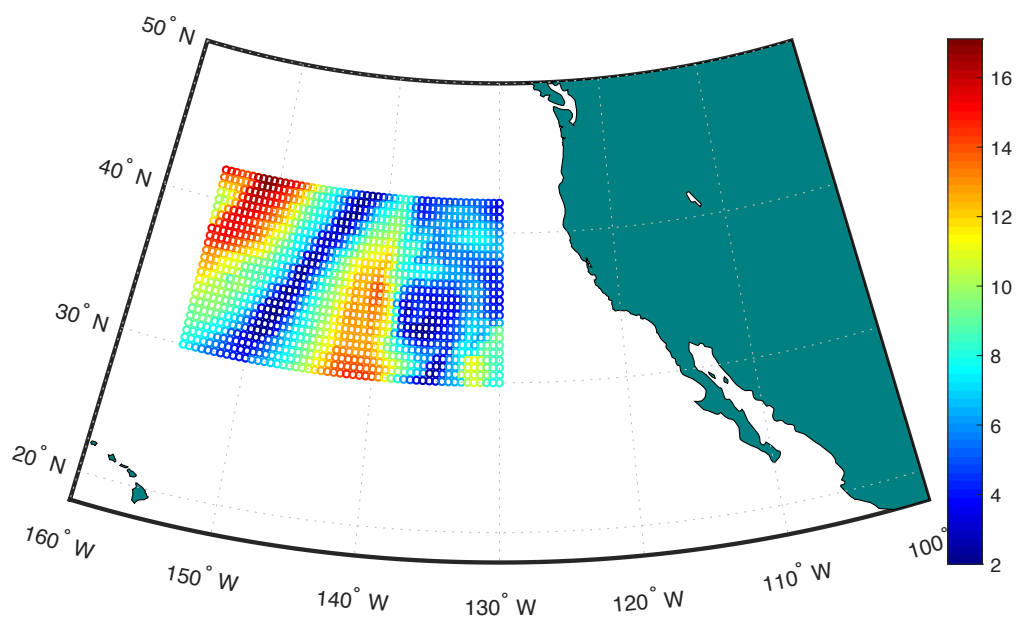


Figure 3.1: Wind data from 2016 in m/s .

Figure 3.2: Wind data from 2017 in m/s .Figure 3.3: Wind data from 2018 in m/s .

3.1.2 Wave data

For the purpose of this thesis, the significant height of combined wind waves and swell data was used as this represents the wave period associated with the most energetic waves in the total wave spectrum at a specific point. Figure 3.4, 3.5 and 3.6 below represent the significant wave height for the GPGP in 2016, 2017 and 2018, respectively.

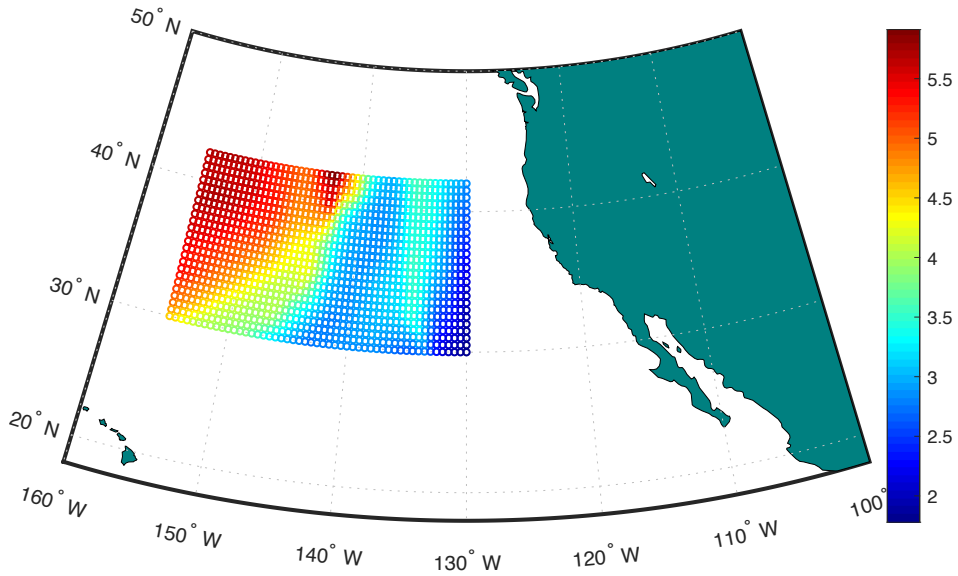


Figure 3.4: Significant wave height data from 2016 in *m*.

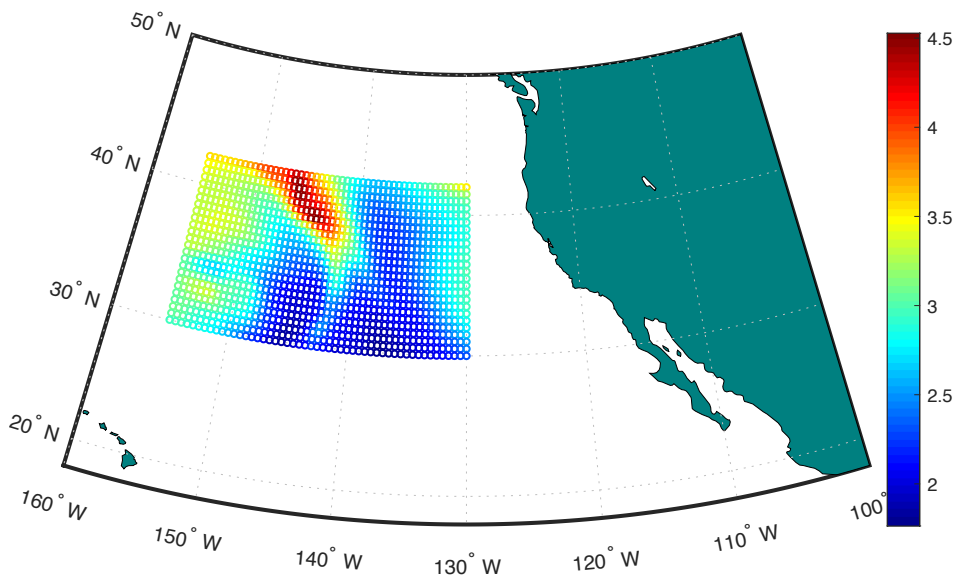


Figure 3.5: Significant wave height data from 2017 in *m*.

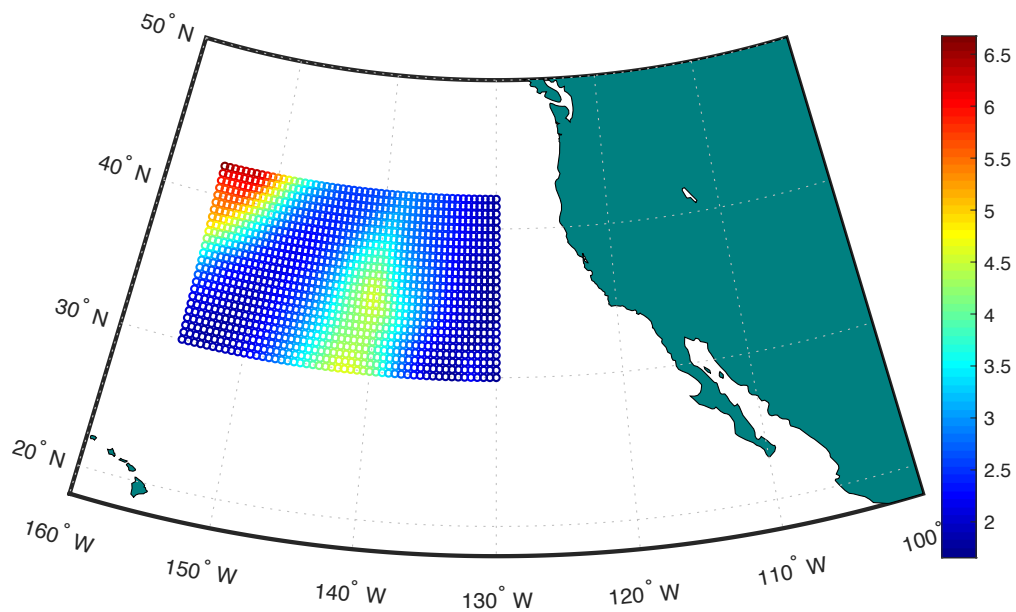


Figure 3.6: Significant wave height data from 2018 in m .

By comparing the wave data with the wind data in Section 3.1.1, a correlation can be seen. Higher wind speed contributes to higher significant wave height in the same locations. The weather data in this chapter is measured at different coordinates in the area of interest. However, as the system will be drifting with the wind, current and waves in the area, the system will not stay at one coordinate for long. As the path of the system is difficult to predict by use of the data available, simplifications had to be made in order to determine the calm periods in the GPGP.

According to the Beaufort Scale, the effect of wind speeds in the range $1.6-3.3 m/s$ results in small short, but pronounced wave. This means that the crests have a glassy appearance but do not break. As the minimum measured wind speed in the period 2016-2018 is $2 m/s$, it is expected that the minimum wave height will be in the range $0.3-0.6 m$ (Britannica Academic, 2017). However, the minimum registered significant height of combined wind waves and swell was found to be $0.8 m$ over the course of the three years of interest. In general, wind generated waves tend to have smaller peak wave periods than swell and it is therefore reasonable to look at a combination of the two.

3.1.3 Weather data summary

For the continuation of this thesis, the minimum wind speed, significant wave height and peak wave period are of interest, as this is assumed to be the period when the system moves too slowly. There was no available data indicating under which exact conditions the system was struggling with retaining the plastic it had accumulated. It was therefore desirable to find and define the "calm periods" where the system is not able to retain the plastic, and it was thus decided to perform future calculations by using minimum registered values to produce conservative results.

As the peak wave period and significant wave height are directly correlated, the peak wave period from the same coordinate and same day was used. The minimum values found in the GPGP from 2016 to 2018 were found by use of the MATLAB script *weather_data.m* in Appendix A.1 and are presented in Table 3.1 below. The wavelength is a function of the wave period and refers to the length between two wave tops.

Table 3.1: Minimum values for the weather data in the GPGP from 2016 to 2018.

| Wind speed [m/s] | Significant wave height, H_s [m] | Peak wave period, T_p [s] | Wavelength, λ [m] |
|----------------------|--|---------------------------------|-------------------------------|
| 2 | 0.8586 | 3.9872 | 24.8213 |

Figure 3.7 below illustrates the definition of height and wavelength of a wave. In addition, the wave depth is defined as the distance from the mean vertical position of a surface particle and will be an important parameter in the concept development phase of this thesis.

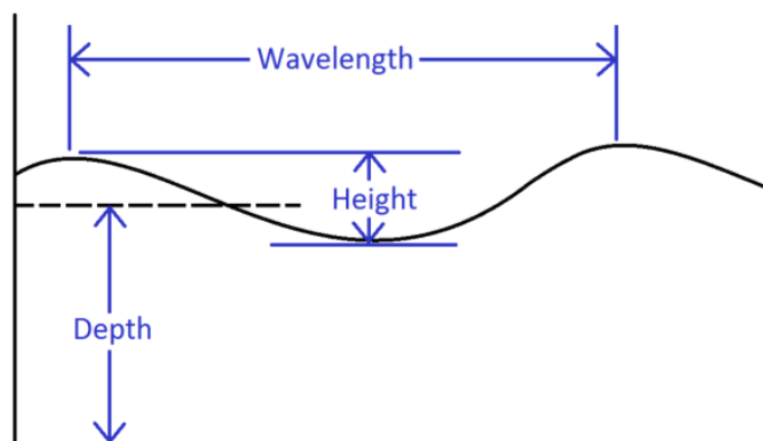


Figure 3.7: Illustration of a wave with height, wavelength and depth (Liu, 2013).

It would have been interesting to follow the system as it drifts in the GPGP and register the weather conditions along the path the system takes. However, as information about the drifting pattern of the system was unavailable, it was decided to find solutions that would be able to operate under the calmest weather conditions.

In order to exploit the natural forces more efficiently, it is relevant to look at solutions that focus on the three parameters that the system is designed to use. This chapter has provided information about the calm weather conditions and will be the basis when looking at solutions going forward. Considering the weather data obtained in this chapter, concepts and ideas were developed and are presented in the following chapter, Chapter 4 - *Concept development*.

Chapter 4

Concept Development

This chapter will discuss concepts to make the Ocean Cleanup's System 001 drift faster under certain conditions. As this is a passive system, i.e. it does not benefit from mechanical propulsion systems, it is relevant to look into methods of increasing the speed while conserving the passiveness of the system.

4.1 Propulsion concepts

As only the part of the floater above water is facing the wind and is therefore directly affected by the wind, a possible solution would be to increase the effective area above the water surface. This would be an attempt to exploit the wind more efficiently under calmer conditions. It was also relevant to look at possible solutions utilising the currents in the area. However, as both the plastic and the system will drift with the current, they will drift with the same relative speed if no other forces are taken into consideration. Further, due to the lack of data about the currents in the area, it was decided not to focus on utilising this force going forward.

A number of propulsion systems were considered in order to find a concept that could contribute to additional propulsion for System 001 under calm conditions. These included flexible and rigid solutions, both above and below the water surface. The concepts considered in this thesis are presented below.

Flexible solutions

The possibilities of using kites or flexible sails were discussed but were rejected as it was discussed whether these solutions would be able to withstand the wind forces induced on flexible constructions during a storm. This conclusion was later confirmed by the Ocean Cleanup themselves in an article published in late May of 2019.

The article presented the possible solutions the organisation had looked at over the past six months. One of the concepts includes the use of flexible sails, which would contribute to an increase of the windage of the system. However, the loads from the sail would be too great during storms with approximately five *tonnes* of force for every *m* of sail. This force would lead the system to capsize and the concept was thus proclaimed not feasible (The Ocean Cleanup, 2019). This idea will however be tested by the Ocean Cleanup later this year by using giant inflatable buoys on the front of the system, which will act as a towing mechanism and propel the system by the force of the wind.

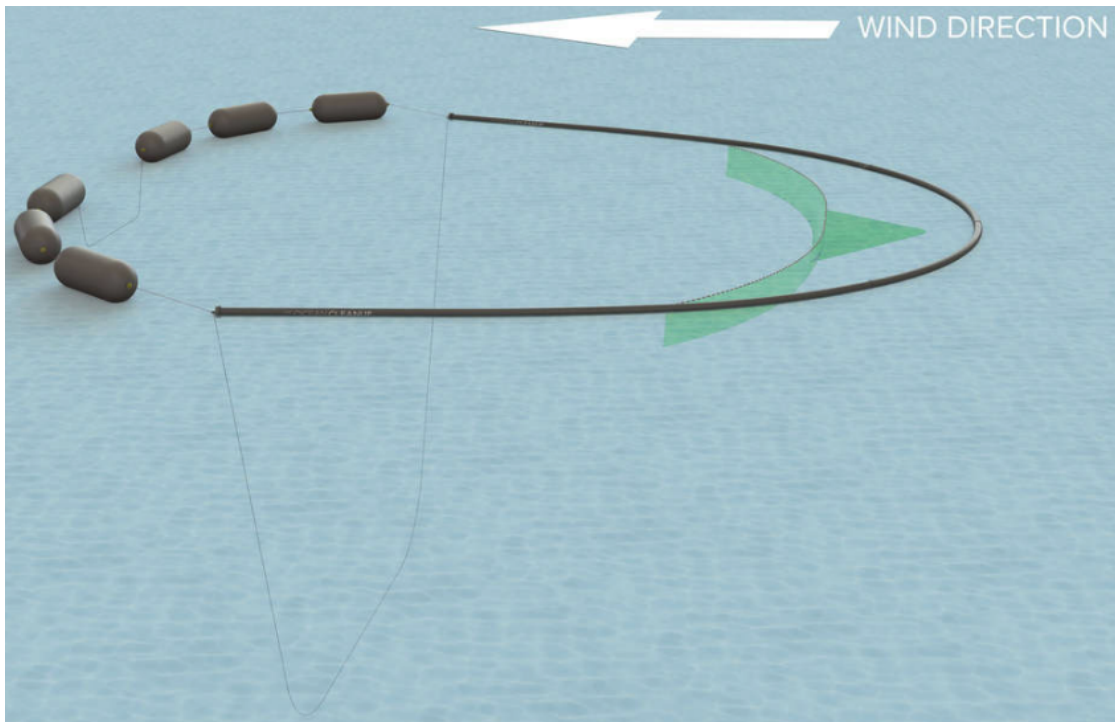


Figure 4.1: Using inflatable buoys as sails to utilise the wind more efficiently (The Ocean Cleanup, 2019).

Slowing down the system

It was also discussed whether a better solution to the retention problem was to slow down the speed of the system, rather than making it go faster. The speed of the system could be decreased enough to drift at a lower speed than the plastic at all times. Maintaining a lower speed than the plastic at all times, and shifting the system 180° , would allow the system to collect plastic and retain it at all times. Although this solution could potentially be an interesting avenue to investigate, it was decided to focus on the objective of the thesis, which includes finding concepts that contribute to additional propulsion.

The article mentioned in the section above, published by the Ocean Cleanup in late May of 2019, looked at a concept similar to the one discussed in this section. By attaching a massive 20-m-diameter parachute-like sea anchor, the system will rotate 180° and slow down sufficiently enough for the plastic to travel faster than the system at all times (The Ocean Cleanup, 2019). Figure 4.2 below illustrates the idea carried out by the Ocean Cleanup.

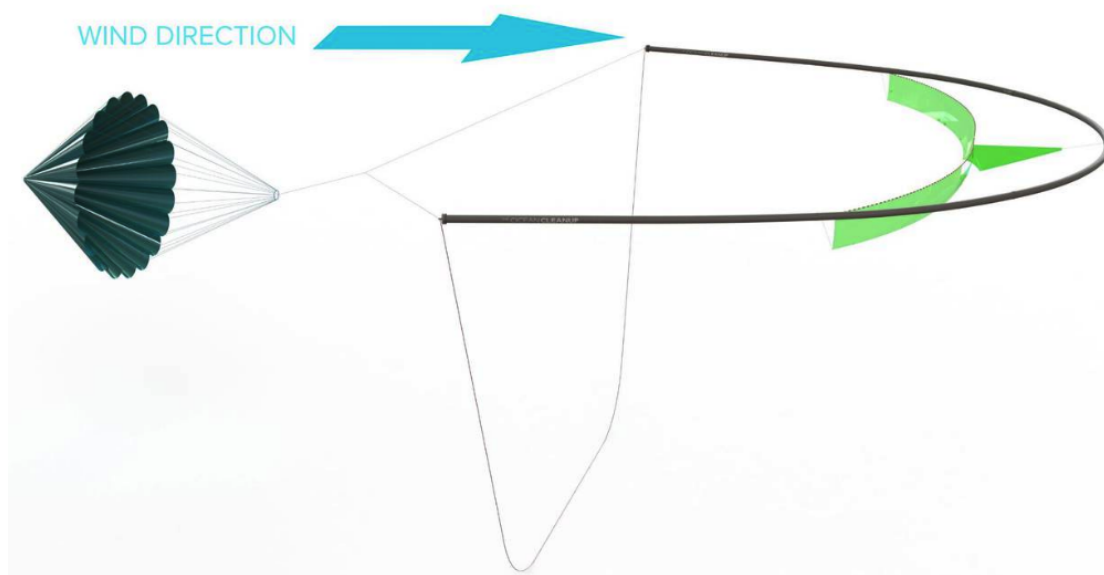


Figure 4.2: Slowing down the system by attaching a parachute-like sea anchor (The Ocean Cleanup, 2019).

Rigid sails and rudders

The use of rigid vertical foils as sails or rudders were discussed as solutions to utilise the wind and currents. The sails and rudders could, for instance, alter their position either by use of solar power, as this is already used for AIS data, or by attaching springs. Figure 4.3 below illustrates the ideas of using vertical foils as sails or rudders to increase the drifting speed of the system.

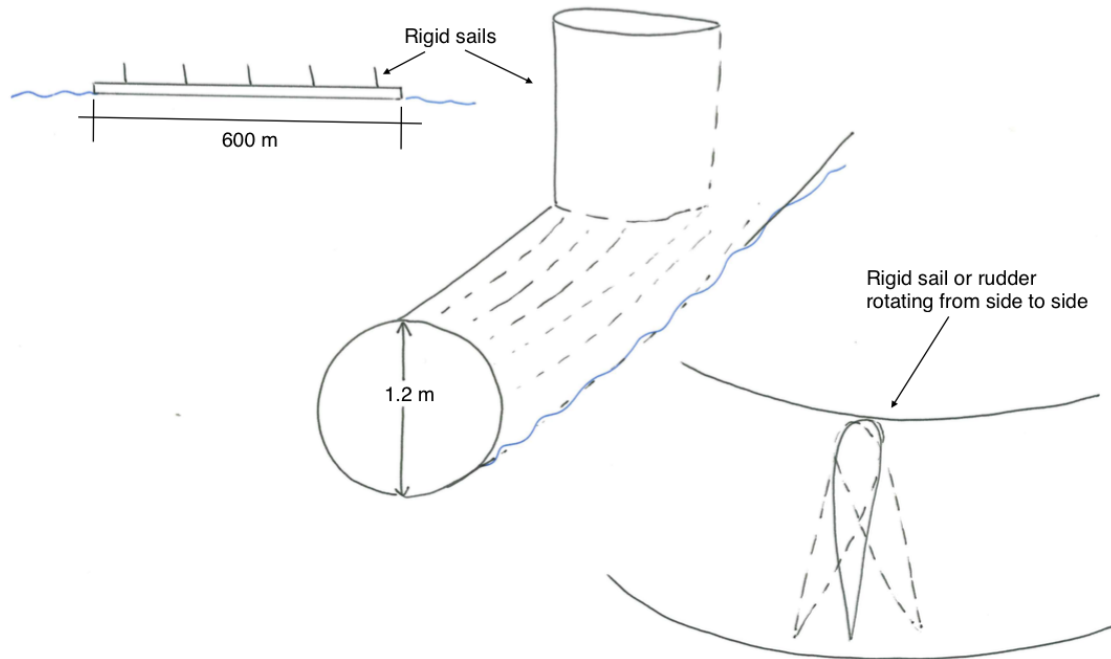


Figure 4.3: Use of rigid vertical foils as sails to utilise the wind or as rudders to utilise the currents.

As this system is dependent on mechanical systems, it was decided to look for other possible ways of utilising foils for additional propulsion, while still conserving the passiveness of the system. These concepts were therefore not prioritised when compared with the idea of using passive horizontal foils in the next section for additional propulsion.

Horizontal foils

The following solution focuses on the exploitation of waves and the movement of surface particles in the GPGP. When it came to concepts that could lead to more efficient exploitation of the wave energy in the area, oscillating foils were an interesting concept to research further. The initial concept idea is illustrated in Figure 4.4 below.

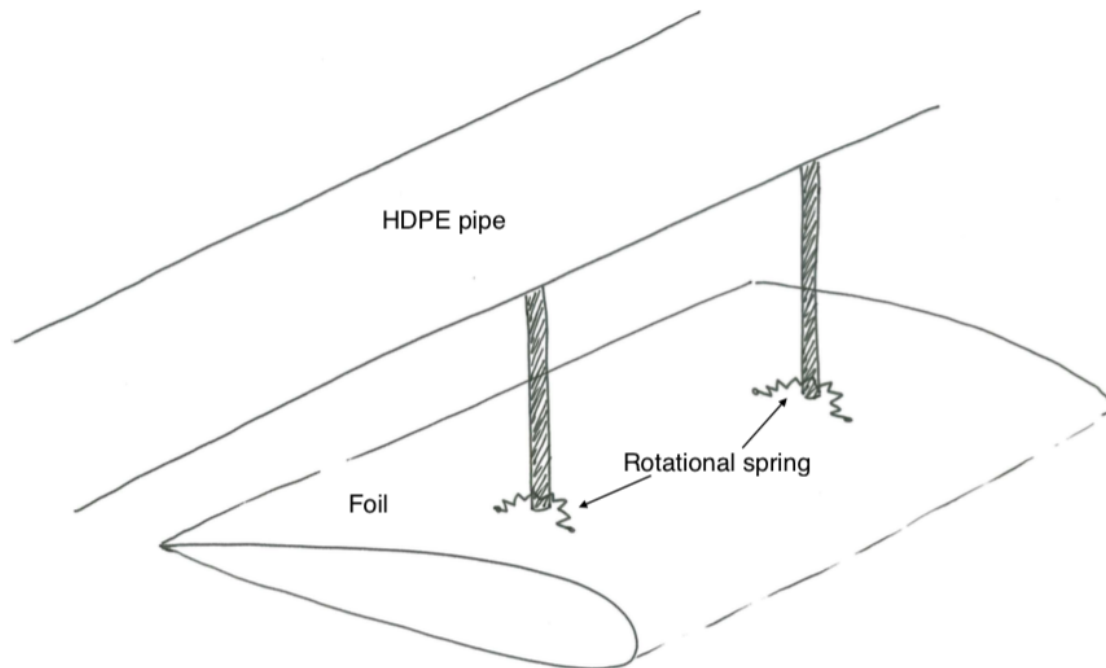


Figure 4.4: Attaching foil with rotational springs under the floater (HDPE pipe). The screen is not included in this illustration.

Going forward, it was decided to focus on one concept to use in the feasibility study. Thus, for the continuation of this thesis, exploiting waves under calm conditions by the use of hydrofoils will be the main focus. The solution will, as mentioned previously, also be based on the criteria that this is a passive system and the possibility of using active propulsion will therefore not be discussed further.

Utilising foils to close off the U-shape

In addition, it was discussed how these foils could be used to minimise the plastic retention problem. One of the possibilities is illustrated in Figure 4.5 below, where the foils are used to close the U-shaped floater so that the plastic is not able to leave the system. Another option was to focus on using the foils to generate additional thrust to maintain a higher speed than the system. The latter option was used further in this thesis.

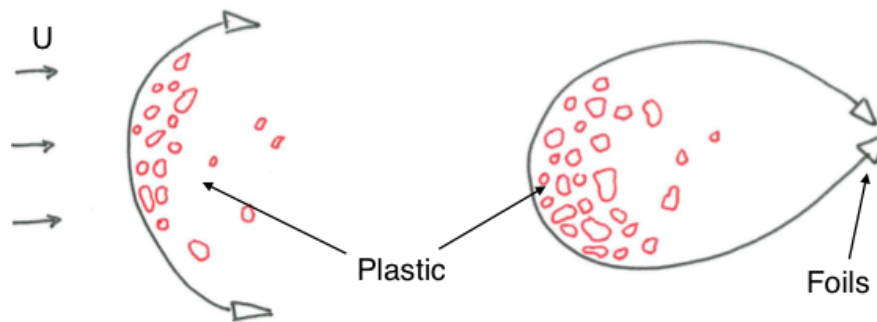


Figure 4.5: Utilising foils to close off the U-shape of the system to avoid plastic escaping under calm weather conditions.

4.2 Foil theory

In order to generate lift on a hydrofoil, the foil must either be cambered or positioned such that there is a difference in angle between the direction of the flow and the foil. This is generally referred to as the angle of attack, α . The magnitude of the lift will depend on the thickness of the foil, the camber and the angle of attack. Figure 4.6 below illustrates the main characteristics of a foil.

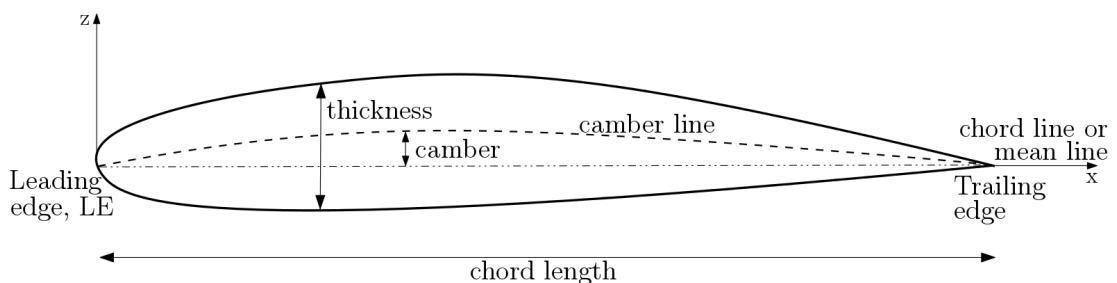


Figure 4.6: 2D foil geometry (Dagestad, 2018).

Foil characteristics

An asymmetric foil will have one suction side and one pressure side. The pressure will be lower than the static pressure on the suction side, while on the pressure side, the pressure will be higher than the static pressure. As a result, the foil is drawn towards the suction side, resulting in lift. Lift force is induced by the circulation of fluid around the foil (Eitzen, 2012). Figure 4.7 below illustrates how circulation occurs on a foil.

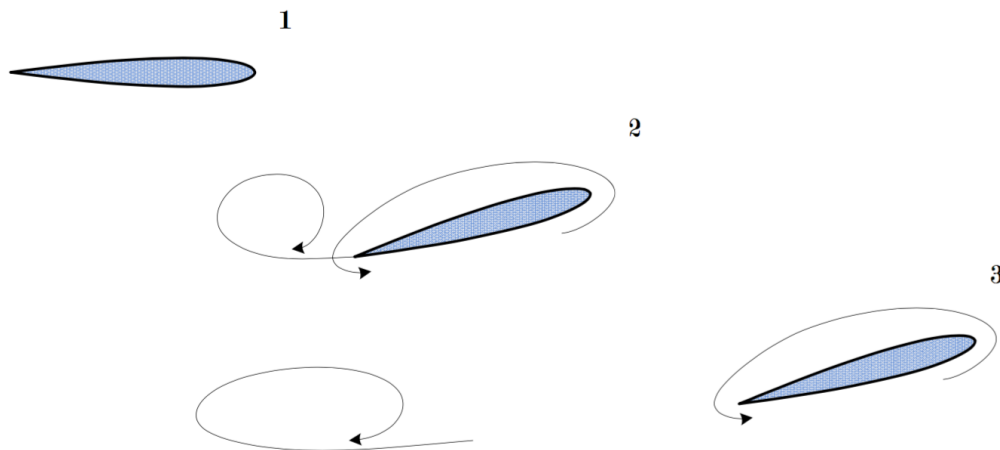


Figure 4.7: Visualisation of the effect of unsteady flow on a foil. 1: No angle of attack and no lift. 2: Instantaneous change in angle of attack and the onset of circulation and vortex-shedding. 3: Steady-state flow and circulation (Eitzen, 2012).

In addition to this force, there will also be a drag force acting in the opposite direction of the foil propagation (Dagestad, 2018). A foil with no camber and zero angle of attack will not generate lift, thus the total circulation around the foil will be zero. However, if a transverse velocity component is imposed in the flow, a circulation will occur and lift will be induced on the foil (Riley, 2015). Figure 4.8 illustrates the effect of the angle of attack and the resulting lift and drag forces, where the lift is normal to the inflow, U , and the drag is parallel.

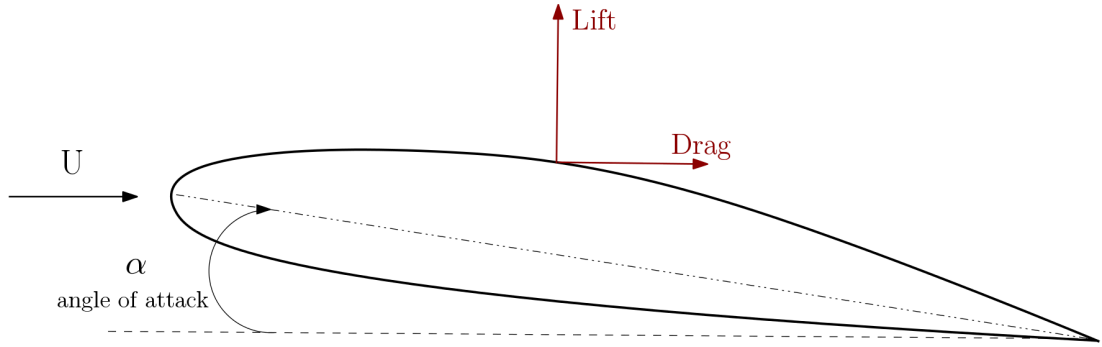


Figure 4.8: 2D foil with angle of attack, α (Dagestad, 2018).

4.2.1 Quasi-static theory

According to quasi-static theory, the effectiveness of a foil can be described by using dimensionless lift and drag coefficients, C_L and C_D . These coefficients are used to calculate the lift and drag forces, L and D . The lift coefficient of the foil can be expressed by using the lift coefficient obtained from to both the camber and the angle of attack, and can be written as $C_L = C_{Lc} + C_{L\alpha}$ (Steen, 2011). In the case of symmetric foils, where the camber is zero, the angle of attack can be expressed as $C_L = C_{L\alpha}$. Equation 4.1 and 4.2 below are used to calculate the lift and drag forces acting on a foil.

$$L = \frac{1}{2}\rho V^2 C_L S \quad (4.1)$$

$$D = \frac{1}{2}\rho V^2 C_D S \quad (4.2)$$

where ρ is the density of seawater, V is the effective inflow on the foil, C_L is the dimensionless lift coefficient, C_D is the dimensionless drag coefficient and S is the area of the foil.

Quasi-static theory considers the instantaneous change in angle of attack. This is visualised in Figure 4.9 below. As seen of the figure, it is more accurate to use unsteady lifting theory as it does not only take into account instantaneous step-functioned angles of attack (Eitzen, 2012).

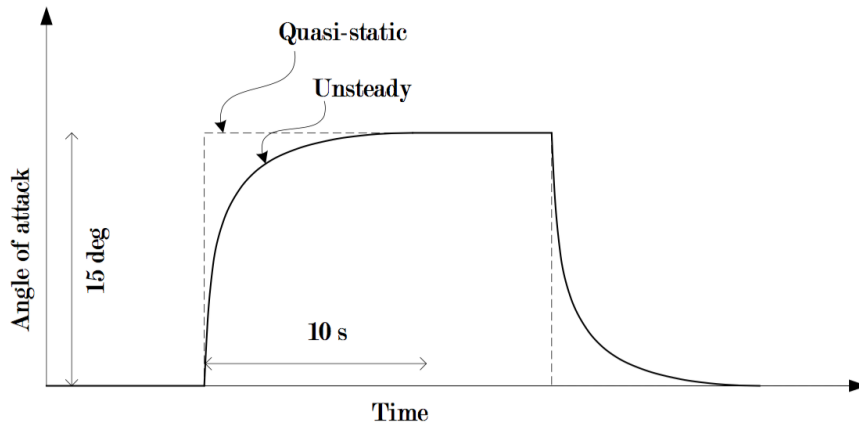


Figure 4.9: Angle of attack on a foil according to quasi-static and unsteady lifting theory (Eitzen, 2012).

In addition to the lift and drag force, there is a thrust force, T , acting in the direction of foil propagation. If the thrust is greater than the drag, the system will be propelled in the direction of the thrust. In order to keep the lift component facing forward, it is desirable to be able to alter the angle of attack of the foil (Mannam, Krishnankutty, & Mallikarjuna, 2014). It is possible to obtain thrust from a hydrofoil in a free stream by oscillating the surface in a direction normal to the stream velocity.

The vortices shed from the trailing edge of a stationary object in a moving fluid are often predictable patterns of eddies and are generally referred to as von Karman vortices (Willis, 2013). These vortices contribute to foil drag. However, at some frequency range, the vortices rotate outward and generate a jet flow aftward, resulting in reversing the drag so that it acts as a thrust in the forward direction. These vortices are referred to as reverse von Karman vortices (Mannam et al., 2014). Figure 4.10 below illustrates the difference in wakes formed behind a stationary cylinder and an oscillating foil. The concepts discussed in the next section are based on the principle of oscillating or flapping foils.

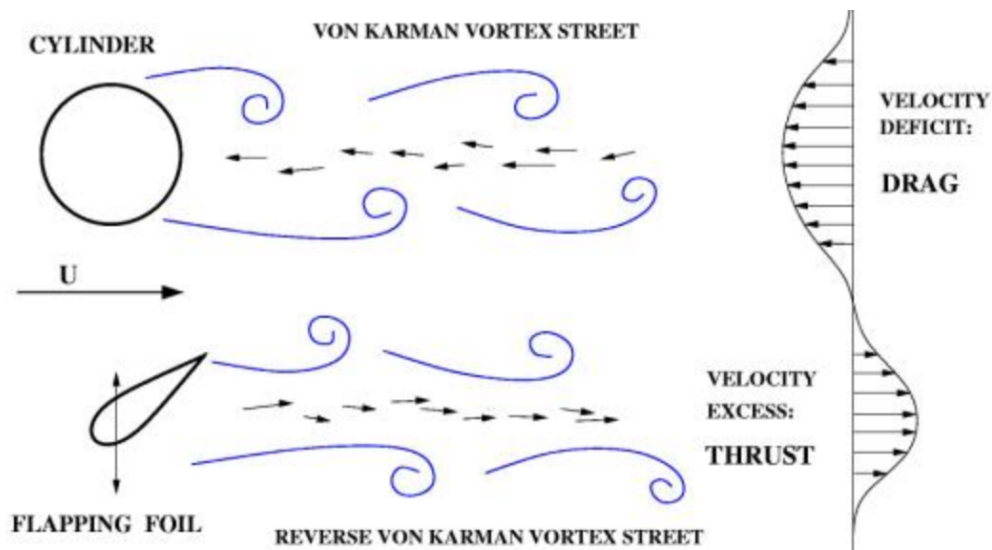


Figure 4.10: Vorticity dynamics in drag versus thrust wakes (Yulin Pan, n.d.).

4.3 Potential concepts

The following concepts represent different ways of utilising the advantages of hydrofoils, while at the same time conserving the passiveness of the system. These concepts were thoroughly investigated before one of the concepts was chosen to research further in the continuity of this thesis.

4.3.1 Wave glider

A wave glider harvests energy from wave and solar power. The concept consists of a submerged glider containing six hinged flat hydrofoils arranged in tandem and a tether connecting the glider to a surface boat (Yang, Shi, Zhou, Guo, & Wang, 2018). Figure 4.11 below illustrates the composition of the different components of the wave glider.

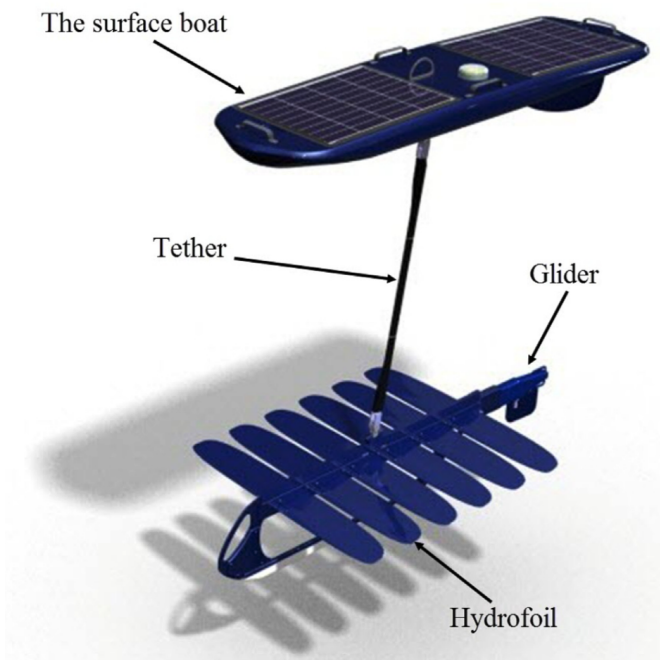


Figure 4.11: Illustration of a wave glider (Yang et al., 2018).

The system makes use of the vertical motion of the waves acting on the parallel wings of the wave glider and then convert this into forward thrust. This conversion will happen as the floaters moves up and down with the waves (Yang et al., 2018). When the boat encounters a wave, it pulls the glider up through the tether, which induces an angle of attack for the hydrofoils to generate a thrust to propel the system forward. As the glider descends from the wave, the hydrofoils flap and produce another thrust force to propel the system (Yang et al., 2018). This is illustrated in Figure 4.12 below. When the rotation angle reaches its maximum value, the torsional force will rotate the torsional spring to restore to its original conditions (Chen, Ge, Yao, & Zheng, 2018).

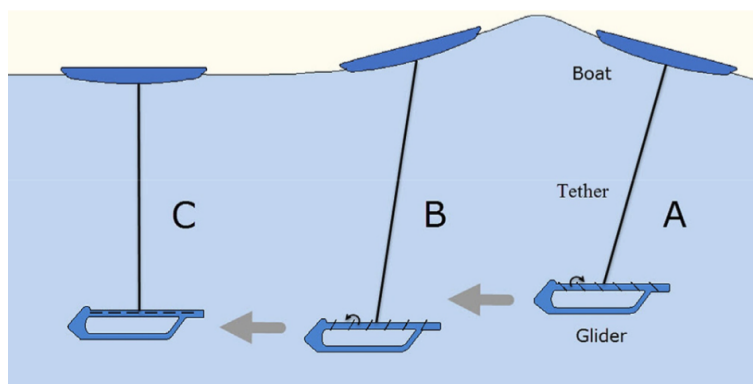


Figure 4.12: Operational mechanism of wave glider (Yang et al., 2018).

According to AUVAC (Autonomous Undersea Vehicle Applications Center), a system like this can create an average speed of 2-3 *kn* (1.03-1.54 *m/s*) of a surface boat with 3.5 *m* LOA, 0.43 *m* height and 0.43 *m* beam (AUVAC, n.d.). However, for flat calm conditions the propulsion is closer to 1 *kn* (0.51 *m/s*). Thus, this is a system that can operate also under calm conditions (Li, Liu, Wang, & She, 2017). Liquid Robotics Inc. also designed a wave glider with a 7 *m* long umbilical cord which was able to maintain a forward speed of 1.5 *kn* (0.77 *m/s*) in seas with 0.3-0.9 *m* waves. The forward speed is dependent on the weight of the glider, the overall buoyancy force of the float and the amplitude of surface waves. With 0 *m* waves, the system was observed to yield speeds of 0.25-0.5 *kn* (0.13-0.26 *m/s*), while 1 *m* waves and higher resulted in speeds exceeding 1.5 *kn* (0.77 *m/s*) (Manley & Willcox, 2010). These observations were made in the Pacific Ocean between California and Hawaii in 2009.

4.3.2 Foils with adjustable flaps

The concept behind flapping foils is to simulate the movement of a dolphin's or a whale's tale movement in the water. This movement is used as propulsion and can be adopted into other systems. The goal is to make boats more fuel efficient by generating propulsion with a flapping foil. A dolphin's tale has a power efficiency of up to 90%, while a conventional propeller only has a power efficiency of 50-60% (Hanley, 2016).

Lift is typically created when the upper surface is more curved than the lower surface or by providing an angle of attack to the flow by tilting the wing/fin. Experiments have indicated that it is more efficient to use flexible flaps than rigid ones. The flexibility enables the flap to have a variable angle of attack along its span (Mannam et al., 2014). It is possible to obtain thrust from a hydrofoil in a free stream by oscillating the surface in a direction normal to the stream velocity. In other words, by reversing the von Karman vortex, thrust can be generated instead of drag.

In the cases where the amplitude is significant at the tail, the swimming is oscillatory and the thrust is primarily generated by the vertical tail flapping of marine mammals. This is similar to the movement of a whale or a dolphin, which is characterised by their streamlined rigid body. The hydromechanical efficiency of a whale has been estimated to be around 85% (Schouveiler, Hover, & Triantafyllou, 2005). Thus, the idea is to mimic aquatic animal fin or tail kinematics to improve the performance and propulsion of the system.

Some hydrofoils are designed with adjustable flaps, which refers to the area closest to the trailing edge. The size of the flap may vary depending on the desired characteristics of the foil. By using trailing edge flaps on foils, the lifting capability of the foil can be enhanced. In addition, a more even pressure distribution can be obtained by altering the camber than by changing the angle of attack of the foil (Dagestad, 2018). Figure 4.13 below represents a foil with different flap sizes. It is also important to investigate different types of foils in order to find the most efficient one. Firstly, it is important that the foil generating the highest thrust and lowest drag is used. Secondly, it is relevant to choose a foil that can have these characteristics without a motor. Having a flap with an angle at the trailing edge will influence the pressure distribution of the whole foil and can be used to control the lift.

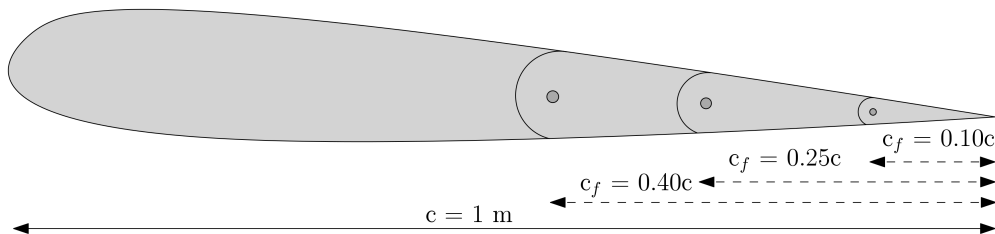


Figure 4.13: Foil with different flap sizes (Dagestad, 2018).

The ability to alter the trailing edge flaps is desirable both to optimise the lift on a foil, making it more efficient, and to avoid cavitation in rolling sea. Thus, the use of trailing edge flaps will provide the foil with camber.

4.3.3 Oscillating foils

In real sea conditions, the system will experience oscillatory motions due to waves. A hydrodynamic analysis of flapping wings located beneath a ship's hull has been carried out by Belibassakis and Politis (Mannam et al., 2014). The results showed that the wing performs combined vertical and angular oscillatory motions in the horizontal arrangement, while travelling at constant forward speed. However, it is common to have an external mechanism controlling the wing pitching motion. The angular motion of the wing about the pivot axis is controlled in order to produce thrust. The use of flapping foils makes it possible to optimise the foil movement to create desirable lift and propulsion forces.

One of the advantages of using oscillating foils includes the mitigation of impact on the environment, as it is less obtrusive and does not have large translational speed. In addition, oscillating foils have structural robustness and high energy harvesting capacity (Zhu, 2012).

An oscillatory foil is able to move in both heave and pitch. Figure 4.14 below illustrates how an oscillating foil can be modelled by using an actuator to drive the heave motion and a torsion spring to resist the moment induced by the hydrodynamic forces.

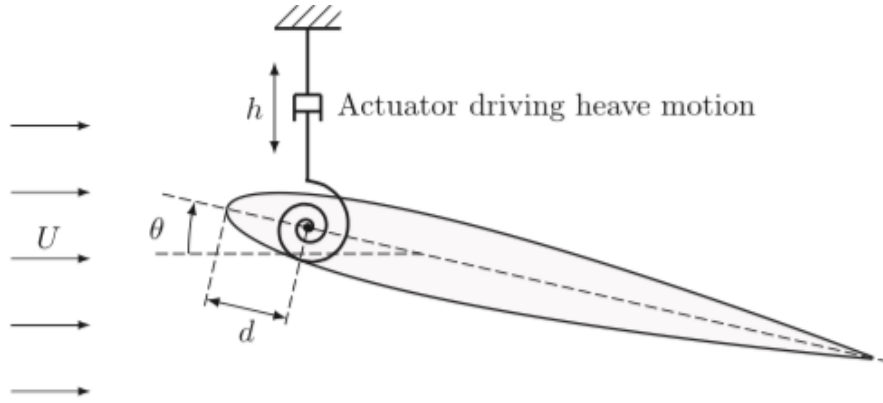


Figure 4.14: Schematic illustration of a semi-active flapping foil with forced heave motion. The pitch angle, $\theta(t)$, is induced by hydrodynamic forces (Thaweewat et al., 2018).

The external forces acting on the foil are the hydrodynamic force and the spring force, and can be written as

$$F_{ext} = F_{hydro} + F_{spring} \quad (4.3)$$

Figure 4.15 illustrates the oscillating motion of the foil during one period. The angle of attack is the angle between the chord line and the incident velocity, i.e., the advance velocity in combination with the heave velocity (Thaweewat et al., 2018). Thus, by altering the angle of attack, the wing can generate lift on either the up or down stroke of the appendage.

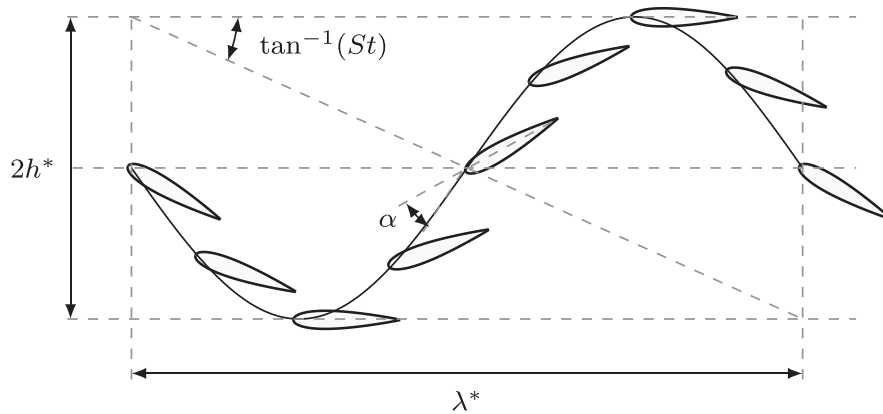


Figure 4.15: Schematic representation of the foil kinematics. The spline represents the path line of pivot location of the foil (Thaweewat et al., 2018).

One of the challenges associated with flapping foils is that they have been used on vessels moving at a much higher speed than System 001. It is therefore of interest to look into the possibility of using this type of technology also in calmer water when the system is travelling at a significantly lower speed. The goal is to generate enough thrust so that the system can maintain travelling at a slightly higher speed than the plastic it is designed to accumulate.

A comparison of the concept behind wave glider, foils with adjustable flaps and oscillating foils indicated that the use of oscillating foils could be more beneficial for the purpose of this thesis. As System 001 at times travel with a very low speed, it is desirable to look at the possibility of generating thrust by oscillating the foil in heave in combination with pitching. It was therefore decided that the use of oscillating foils could be more beneficial than using foils with adjustable flaps. Although wave glider has shown good results for use on smaller floats designed as boats, it was desirable to focus on the use of single oscillating foils for the continuation of this thesis.

Chapter 5

Modelling

This chapter will present the model used in this thesis to determine the feasibility of using oscillating foils to generate thrust under calm conditions. The model is based on multiple assumptions and simplifications. These will be presented as they are taken into use.

5.1 Wave motions

According to the weather data obtained in Chapter 3 and presented in Tabel 3.1, the lowest recorded significant wave height, H_s , is 0.8586 *m* and the peak wave period, T_p , corresponding to this wave height was found to be 3.9872 *s*. For the purpose of this report, harmonic non-damped regular waves were used to calculate the feasibility of using oscillating foils to generate propulsion.

5.1.1 Particle velocity

Understanding the system's movement in waves can be a challenging and comprehensive task. Thus, some simplifications had to be made. As waves consist of fluid particles in motion, it was assumed that the motions of the system are connected with the particle motion on the surface of the wave. Figure 5.1 below illustrates the orbital motion of particles in a fluid during one period, T_s .

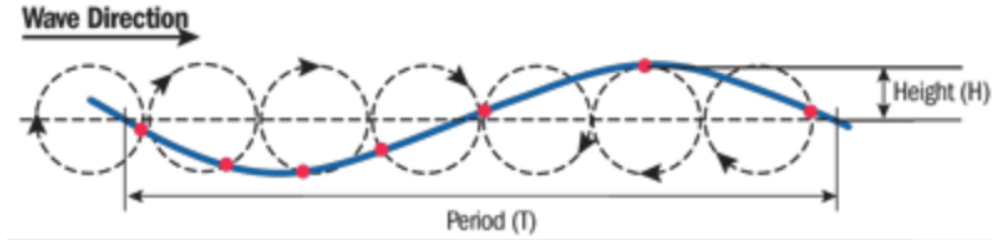


Figure 5.1: Illustration of the path a particle takes on the surface in waves.

Stokes waves

A consequence of the non-linearity of waves is that the fluid particles do not move in closed paths but will slowly drift in the propagation direction of the wave. Stokes drift is the result of the horizontal velocity component of a particle on the top of the orbit being slightly larger than the velocity at the bottom of the orbit (Krogstad & Arntsen, 2000). The net result is therefore a slight displacement along the wave direction as seen in Figure 5.2 below.

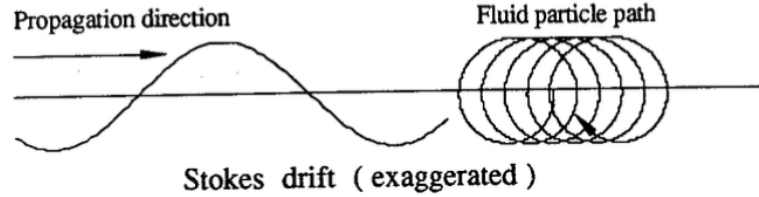


Figure 5.2: Stokes drift particle displacement (Krogstad & Arntsen, 2000).

Stokes horizontal net drift velocity can be described by the following equation:

$$U = c_w k^2 \zeta_a^2 e^{2kz_1} \quad (5.1)$$

and

$$c_w = \sqrt{\frac{g}{k}} \quad (5.2)$$

where $k = 2\pi/\lambda = \omega^2/g$, $\lambda = gT_s^2/2\pi$ and $\omega = 2\pi/T_s$, and where T_s = wave period, λ = wavelength and ζ_a = wave amplitude. In addition, z_1 is the mean vertical position of the fluid particle during a wave cycle, i.e. when there are no waves (Myrhaug, 2006).

Vertical particle velocity

Linear theory implies that the velocity potential is proportional to the wave amplitude. The vertical particle velocity, w , as a function of t can be expressed by the following equation:

$$w = \omega \zeta_a e^{kz} \cos(\omega t - kx_s) \quad (5.3)$$

Stokes drift will decrease as the depth increases. Figure 5.3 illustrates how currents affect the displacement of fluid particles with increasing depth.

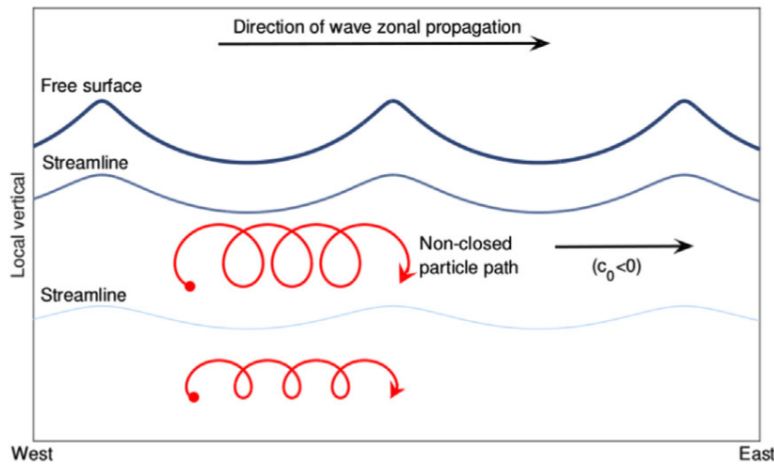


Figure 5.3: The effect of Stokes drift in the vertical direction (Henry, 2019).

Particle velocity at depth $\lambda/2$

According to Pettersen (2007), the effect of the wave motions on the surface is negligible at a depth of $\lambda/2$. Thus, for the purpose of this report, water at this depth will be considered still. Figure 5.4 below illustrates the decrease in orbit radius with increasing depth to the depth of $\lambda/2$. In deep water, the orbital radius decreases as the particle velocities decrease with distance to the surface. The wavelength determines the size of the orbit, while the depth determines the shape of the orbit.

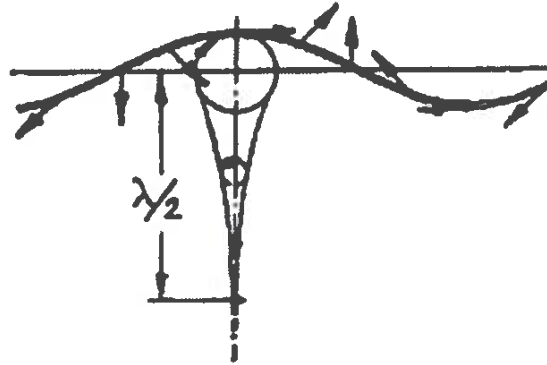


Figure 5.4: Water particle orbit in deep water (Pettersen, 2007).

5.2 System movements

For the purpose of this thesis, the floater is assumed to follow the particle movement on the surface. Thus, the system will drift at the same velocity as Stokes net drift from Equation 5.1. This assumption does however not take into consideration the drag of the submerged section of the system, such as the screen. It does not take into account the effect of wind or currents either, and it is therefore important to keep in mind that this is a simplification implemented for the purpose of this model.

5.2.1 Relative movement between floater and screen

Further, it was assumed that the floater would not pitch with the waves and that the screen would constantly be vertical. This will however not be the case in real life. The effect of applying degrees of freedom to the system is briefly discussed in Chapter 9 - *Further work*. In other words, the system will heave with the waves and project this movement directly down onto the foil attached under the system. Thus, the focus going forward with this report will further be limited to the movement of the foil alone and the thrust it is able to generate under the given weather conditions. Thus, the model will not take the rest of the system into consideration (i.e. the floater and screen), except for the induced heave force on the foil from the heaving motion of the floater in the surface waves.

5.2.2 Foil characteristics

Depth of foil placement

In order to induce the force from the floater's heaving motion onto the foil, the foil should be placed at a depth where the wave motions have little effect as mentioned in Section 5.1.1. From the wave period obtained from the weather data in Chapter 3, the wavelength, λ was found to be approximately 24 m. Thus, by placing the foil at a depth of $\lambda/2 = 12$ m, the foil will have to displace the water as it moves up and down with the waves. This will further result in a hydrodynamic force altering between acting on the upper and lower surface of the foil.

Effective inflow and angles

As U is assumed constant along the wave, while the vertical velocity of the foil, \dot{h} , varies with t , both the effective inflow velocity, V , and the angle between the horizontal direction and the effective inflow, ϕ , will vary with t . Furthermore, as Stokes net drift velocity is small relative to the vertical velocity, the vertical velocity becomes the dominating factor and contributes to a $\phi \approx 90^\circ$. The force from the effective inflow acts in the pivot point and the velocity can be expressed by the following equation:

$$V(t) = \sqrt{U^2 + \dot{h}(t)^2} \quad (5.4)$$

where $\dot{h}(t)$ is the vertical heave velocity, U is the net Stokes drift and is assumed constant for the purpose of this thesis. As the wave passes the system, the vertical velocity will alter between positive and negative values. This results in the effective inflow velocity altering between acting on the upper and the lower side of the foil, making it heave up and down. An illustration of the effective inflow velocity acting on the foil can be seen in Figure 5.5 below. Figure 5.6 defines the angle of attack, $\alpha(t)$, the pitch angle, $\theta(t)$, and the inflow angle $\phi(t)$, which will be relevant for the model set-up.

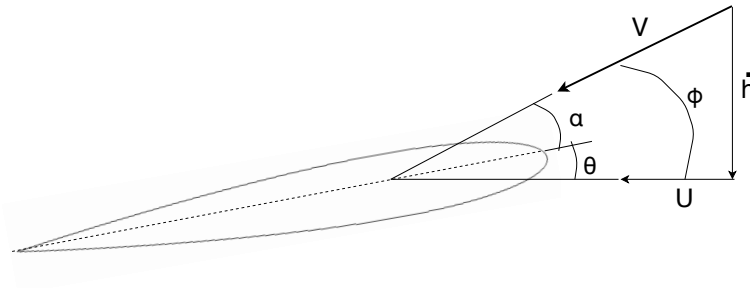
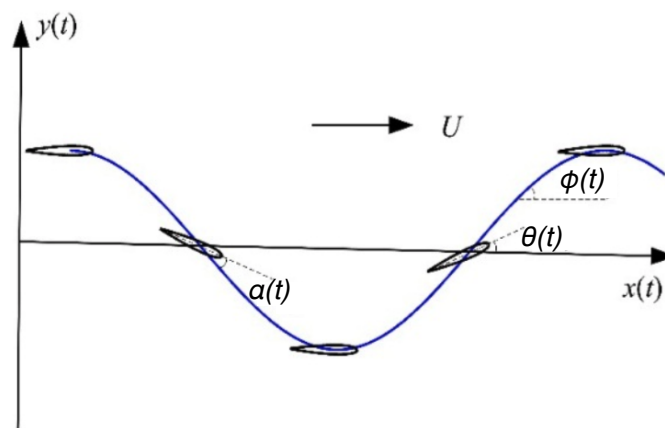


Figure 5.5: Effective inflow velocity on foil.

Figure 5.6: Definition of angles $\alpha(t)$, $\theta(t)$ and $\phi(t)$.

The inflow angle is dependent on both the horizontal drift velocity and the vertical heave velocity, and can be expressed as:

$$\phi(t) = \tan^{-1}\left(\frac{\dot{h}(t)}{U}\right) \quad (5.5)$$

From this, the equation for the angle of attack and the pitch angle as functions of the inflow angle can be obtained (Simpson, Licht, Hover, & Triantafyllou, 2008).

$$\alpha(t) = \phi(t) - \theta(t) \quad (5.6)$$

Figure 5.7 to the right illustrates the definition of angle of attack for a pitching foil with vertical inflow.

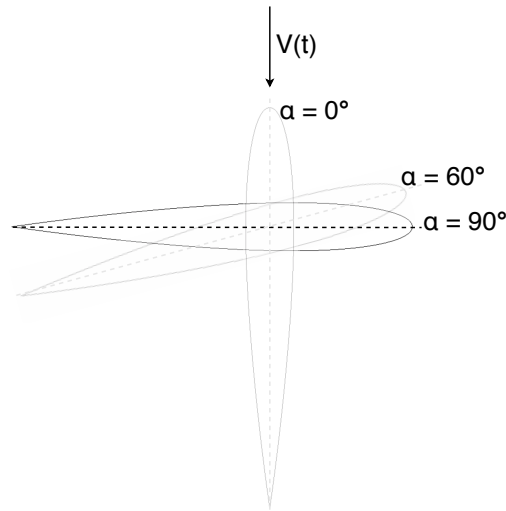


Figure 5.7: Angles of attack relative to vertical inflow.

Foil profiles

In order to generate equal amounts of thrust on both the up-stroke and down-stroke, it was reasonable to look at the possibilities of using a symmetric foil. For the purpose of this thesis, a NACA 0012 profile was used. However, it would also be relevant to compare the results from using this profile with other foil profiles, such as NACA 0009 and NACA 0006 (Hoerner, 1985). This is discussed further in Chapter 9 - *Further work*.

5.3 Oscillation

In order to generate thrust, the foil will need to both heave and pitch. For simplification, it can be assumed that the foil will move with the same heaving motion as the floater on the water surface. The foil will pitch as a result of the displacement of water when heaving.

A system with self-sustained pitching and heaving motions relies on flow-induced instabilities to generate oscillatory motions in the heaving and pitching direction. This will contribute to simplifying the mechanical design of the system as no actuation system is needed. In most of the existing studies, it is assumed that the foil undergoes sinusoidal motions in both heave and pitch direction. The following equations can be used to describe the heaving and pitching motion, respectively (Xiao & Zhu, 2014):

$$h = h_0 \sin(\omega t) \quad (5.7)$$

and

$$\theta = \theta_0 \sin(\omega t + \psi) \quad (5.8)$$

where h_0 is the initial foil position, θ_0 is the initial pitch position and ψ is the phase difference between the heave and pitch motion and is, in most of the cases reported in literature, often an angle of 90° as this provides the highest efficiency. This will, however, depend on the pivot point of the foil (Duarte, 2011). It has however also been reported that smaller phase angles have advantages too.

As the center of fluid force usually occurs at approximately $x = c/4$ from the leading edge, placing the pivot point at $x = c/4$ mitigates the energy expenditure to generate pitching motions (Xiao & Zhu, 2014). It is therefore desirable to place the pivot point closer to the leading edge (LE) to avoid this. Figure 5.8 below illustrates the phase difference between heaving and pitching.

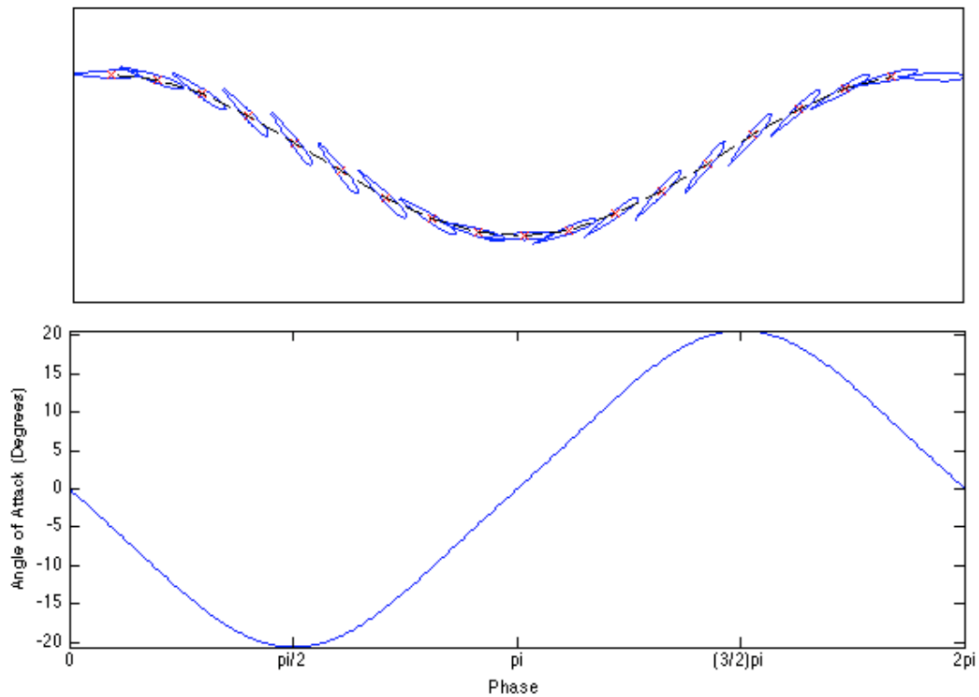


Figure 5.8: Phase difference between heave, h , and pitch, θ , when $\psi = 90^\circ$ (Simpson et al., 2008).

5.3.1 Pitching

The purpose of the pitching foil is to ensure that the foil does not operate with angles of attack that are too large. As the angle of attack increases, so does the lift until the flow separates from the flow on the suction side of the foil, resulting in stall. This is illustrated in Figure 5.9 After reaching this point, the lift will decrease rapidly. The angle at which the foil is subject to stalling is dependent on the foil type chosen (Riley, 2015).

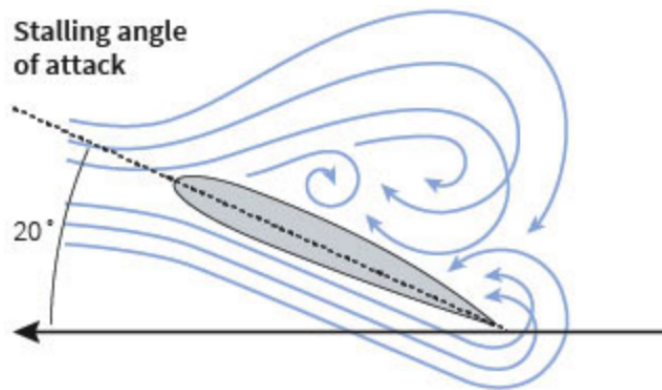


Figure 5.9: A foil experiencing stall will no longer produce lift. This often occurs with angles of attack around 20° (Corones, 2015).

For the purpose of this thesis, the foils are installed with passive pitch control where the pitching angle is controlled by a rotational spring at the pivot point of the foil. Firstly, it is desirable to maintain the simplicity of the system. Secondly, it is cheaper than using an active pitching foil and it also has the benefit of not needing energy supply in order to control the pitching motion. In addition, it is more efficient than using fixed pitching with regards to thrust generation.

In this model, the foil should be able to pitch 180° , i.e. from -90° to $+90^\circ$, assuming 0° pitch when the foil is horizontal. Figure 5.10 illustrates how the foil will be able to pitch in this model.

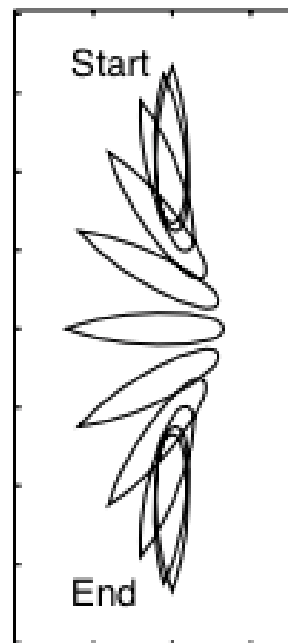


Figure 5.10: Foil pitching in a range of 180° from -90° to $+90^\circ$ (Read et al., 2003).

By inducing a hydrodynamic moment around the foil pitching axis, hydrodynamic forces are imposed on the foil at all times. This moment will cause the foil to rotate towards a smaller angle of attack and the rotation will be determined by the spring stiffness and the location of the pivot point (Riley, 2015). When in equilibrium, the foil will stop pitching.

By using Equation 5.8 to determine the pitch motion of the foil, a 90° phase difference can be seen. This is illustrated in Figure 5.11 below. By only taking into consideration the induced vertical velocity on the foil from the heave motion, the angle of attack becomes a function of the inflow angle at $\phi = 90^\circ$, and the pitch angle, $\theta(t)$, through Equation 5.6. It is however not realistic that the foil will operate at pitch angles of 90° as the foil most likely would benefit from operating at lower pitching angles. This will be investigated further in this thesis.

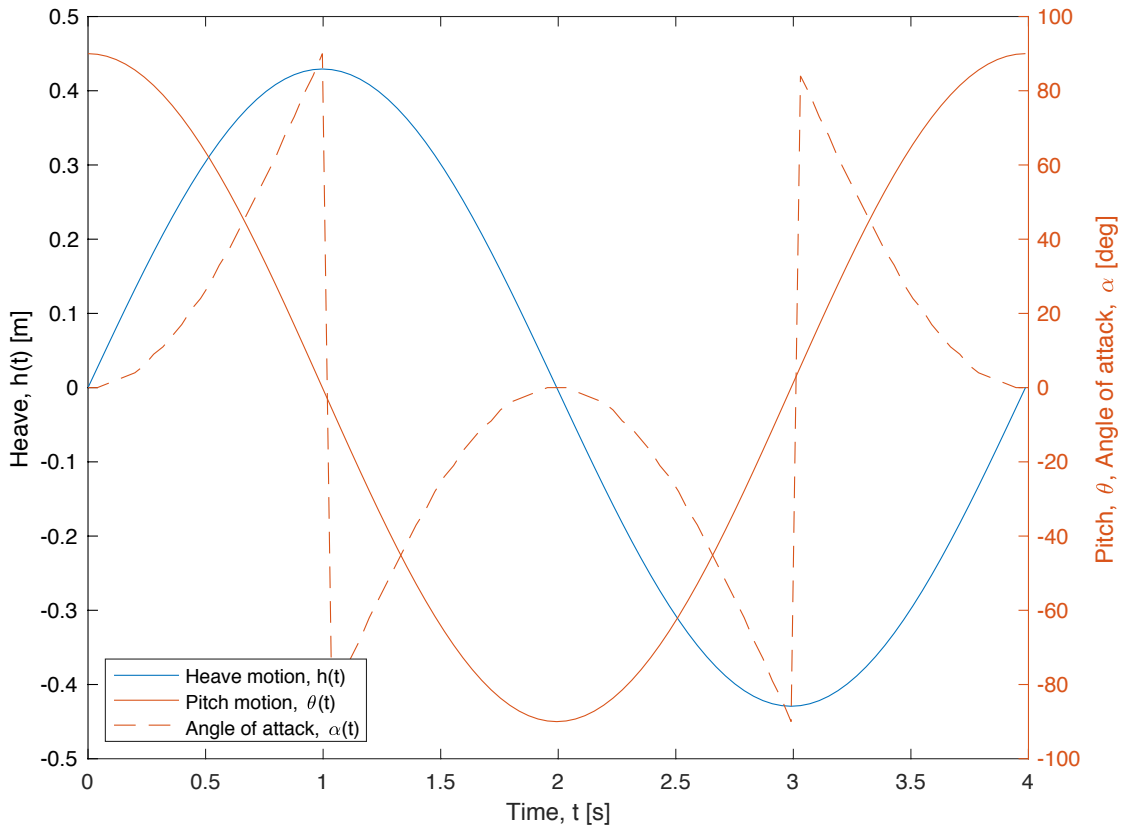


Figure 5.11: Phase difference between the heave motion (—) and pitch motion(—). The angle of attack is a function of the pitch angle (- -).

Pitching-moment characteristics

The pitching moment is imposed by both the lift force and added mass forces. The lift force will, for small angles of attack, act in the quarter-chord point, measured from the leading edge. Added mass forces act in the half-chord point of the foil (Riley, 2015). Thus, the hydrodynamic moment of the foil can be expressed as:

$$\begin{aligned} M_{hydro}(t) &= F_A \cdot (x_a - x_p) \cdot \cos(\theta) \\ &+ D \cdot \sin(\phi) \cdot (x_f - x_p) \cdot \cos(\theta) \\ &+ L \cdot \cos(\phi) \cdot (x_f - x_p) \cdot \cos(\theta) \end{aligned} \quad (5.9)$$

where F_A is the added mass force acting on the foil, x_a is the position along the foil chord where the added mass acts, x_f is the position along the foil chord where the drag force acts and x_p is the pivot point. Position x_a and x_p is illustrated in Figure 5.12 below. L and D are calculated by use of Equation 4.1 and 4.2 in Section 4.2.1, while F_A is calculated by use of the equations presented in Section 5.3.3 below.

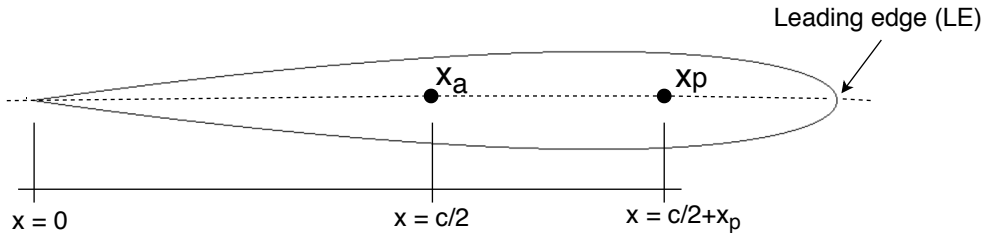


Figure 5.12: Pivot point position. Measured from $x_a = c/2$.

5.3.2 Heaving

The heaving motion of the foil, combined with the pitching, will result in a linearised vertical velocity of the foil, denoted w_{rel} (Hauge, 2013). Using unsteady foil theory, the linearised vertical velocity can be expressed as:

$$w_{rel}(t) = w(t) + \dot{h}(t) - U \cdot \theta(t) \quad (5.10)$$

where $w(t)$ is the vertical particle velocity and $\dot{h}(t)$ is the heave velocity. $\theta(t)$ is also a function of time, while the net horizontal velocity, U , is constant (Eitzen, 2012). As the foil is placed at a depth where the particle velocity is negligible, the term $w(t)$ is zero.

5.3.3 Added mass

This model considers foils with negligible mass, i.e., the mass is insignificant compared with the added mass. Thus, the added mass resulting from the displacement of water as the foil moves up and down has to be taken into consideration. This is done by using the projected chord length of the foil, c_{proj} , which is the length of the 2D plate projected onto the horizontal plane. For a foil oscillating in both heave and pitch, the projected chord length will be $c_{proj} = c \cdot \cos(\theta)$, where c is the chord length of the foil. The projected chord length will be time dependent and may be significantly less than c for large pitch angles (Hauge, 2013).

For a foil, it is relevant to use the added mass coefficient of a cylinder. Figure 5.13 includes the analytical added mass coefficients for a cylinder in infinite fluid.


| Body shape | | Direction of motion | C_A | | V_R |
|-------------------------|---|---------------------|----------|-------|-------------|
| | | | $b/2a$ | C_A | |
| Right circular cylinder |  | Vertical | 1.2 | 0.62 | $\pi a^2 b$ |
| | | | 2.5 | 0.78 | |
| | | | 5.0 | 0.90 | |
| | | | 9.0 | 0.96 | |
| | | | ∞ | 1.00 | |

Figure 5.13: Analytical added mass coefficient for 3D bodies in infinite fluid (DNV GL, 2017).

In this model, $a = c_{proj}/2$ and b is the span of the foil. The added mass can further be written as follows:

$$m_A = \rho C_A V_R \quad (5.11)$$

where C_A is the added mass coefficient and V_R is reference volume (DNV GL, 2017). Using the reference volume of a cylinder gives $V_R = \pi a^2 b$. The non-dimensional added mass coefficient is set to be $C_A = 0.7$ as $b/2a = 2$. This gives:

$$m_A = \frac{1}{4} \cdot \rho \cdot 0.7 \cdot \pi c_{proj}^2 b = \rho \cdot 0.7 \cdot \pi a^2 b \quad (5.12)$$

The added mass in heave is vertical and proportional with the vertical velocity, $w(t)$. It will oscillate with the same frequency as the foil and can be written as:

$$F_A = m_A \cdot (\dot{w} - \ddot{h}) \quad (5.13)$$

where \dot{w} is the vertical particle acceleration and \ddot{h} is the vertical heave acceleration of the foil.

5.3.4 Spring stiffness

In order for the foil to stop pitching, moment equilibrium must be achieved. This is accomplished when the following equation is fulfilled:

$$M_{hydro} = M_{spring} \quad (5.14)$$

where

$$M_{spring} = k_s \cdot \theta \quad (5.15)$$

M_{hydro} is found from Equation 5.9, k_s is the spring stiffness and θ is the pitch angle. The spring stiffness controls the pitching of the foil. By choosing a fixed spring stiffness, there is a danger that the stiffness chosen will be too large and the foil will not pitch sufficiently. On the other hand, choosing a foil with a stiffness that is too small will make the foil pitch too much, making the angles of attack smaller than optimal (Riley, 2015). For the purpose of the calculations in this thesis, the foils will be fitted with only one rotational spring. In real life, it could be favourable to use multiple springs. In this thesis, the spring stiffness will be optimized for a particular sea state.

5.4 Iteration process

Finally, the model will be set up as an iteration process to find the desirable spring stiffness, k_s and pivot point, x_p . This is done by finding the moment equilibrium between the hydrodynamic moment and spring induced moment ($M_{hydro} = M_{spring}$) in Equation 5.14. The following equation is an expansion of Equation 5.14.

$$\begin{aligned}
 & m_A(\alpha)\ddot{h}(t) \cdot (x_a - x_p) \cdot \cos(\theta) \\
 & + \frac{1}{2}\rho V^2 C_D(\alpha) S \cdot \sin(\phi) \cdot (x_f - x_p) \cdot \cos(\theta) \\
 & + \frac{1}{2}\rho V^2 C_L(\alpha) S \cdot \cos(\phi) \cdot (x_f - x_p) \cdot \cos(\theta) = k_s \cdot \theta
 \end{aligned} \tag{5.16}$$

This equilibrium should be fulfilled at each time instant for a fixed spring stiffness and pivot point. When equilibrium is achieved, the thrust at each time step can be calculated.

5.5 Assumptions

The following hydrodynamic assumptions were made for the purpose of this model:

- Damping forces on the foil were neglected. This was due to the absence of experimental tests.
- Cavitation and ventilation will not occur on the foil due to low speeds. It is therefore not discussed further in this thesis.
- Assumptions regarding the center of hydrodynamic forces had to be made as the foil will be pitching with large angles of attack. However, it should be noted that these points will change as the foil pitches and is dependent on multiple parameters.

5.6 Current force on System 001

In addition to setting up a model for the hydrofoils used for this concept, it was relevant to look at the effect of the rest of the system, i.e. the floater and the screen, on the total thrust. This section will describe how the drag forces acting on System 001 are modelled. The model design has been simplified in order to obtain an estimate for total drag on the system.

5.6.1 Force on floater

The first assumption that will be made with regard to the floater is that it will be above water. Firstly, the part of the cylinder that will be submerged will vary with the waves and is therefore not constant. Secondly, as the screen will be the main contributor to the drag of the system in waves, it is reasonable to assume that the drag contribution from the floater is much smaller than the drag contribution from the screen. Figure 5.14 below illustrates three different situations that the floater may experience in real life. In addition, the Ocean Cleanup has stated that no plastic has been observed lost due to overtopping. Thus, for the purpose of this model, it will be assumed that the floater is non-submerged, presented as number 3 in the figure below (White, 2011).

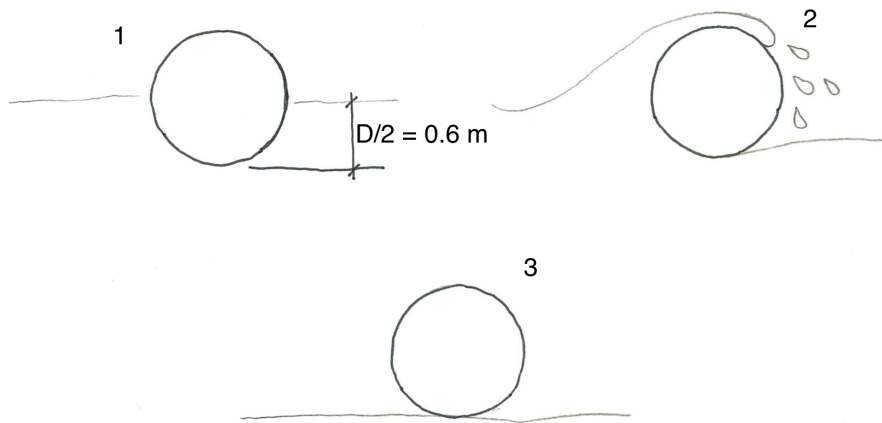


Figure 5.14: Floater position relative to the surface. 1: Semi-submerged floater. 2: Splashing wave over the floater (overtopping). 3: Non-submerged floater.

5.6.2 Forces on screen

According to the Ocean Cleanup, the screen used in System 001 is made of non-permeable material (Slat et al., 2014). Thus, the solidity of the screen, i.e. the ratio between the area covered by the threads in the screen and the total area of the screen, is assumed to be close to 1. As most of the water will move under the screen instead of through it, this model assumes the screen to act as a flat plate. In addition, as the system collects more and more plastic, the flow through the screen will decrease. Figure 5.15 below illustrates the streamlines passing under the screen.

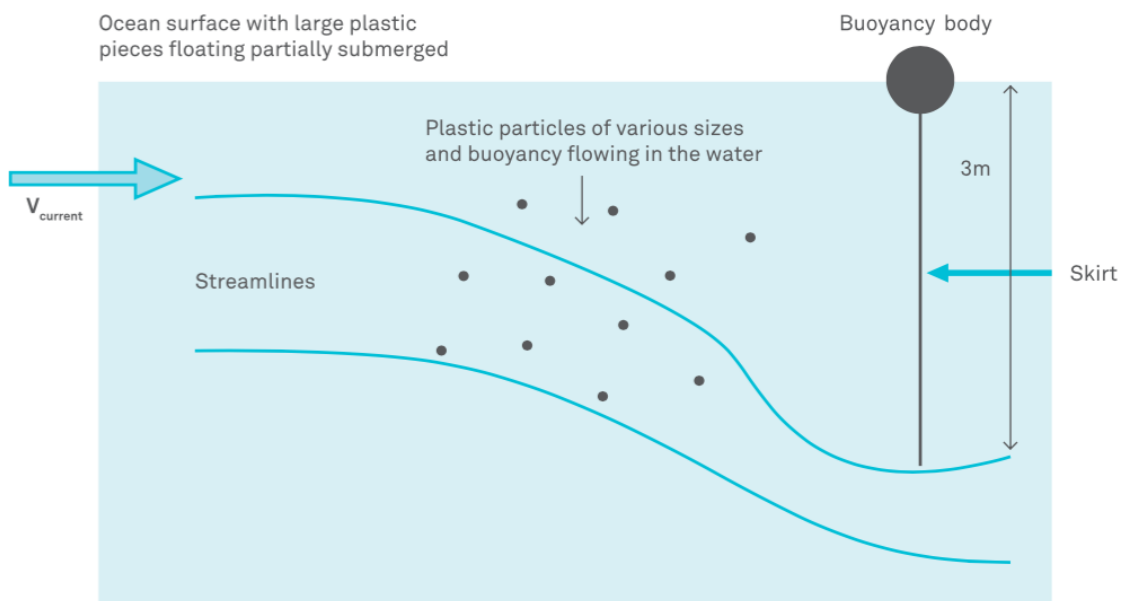


Figure 5.15: Streamlines passing under the system due to the use of non-permeable material (Slat et al., 2014).

In order to calculate the drag forces acting on the screen, the system is assumed to be vertical at all times. In real life, the system will most likely pitch as a result of the foil dragging it along. However, this is not taken into consideration in this model. The drag is calculated by looking at a flat plate in a free stream and dividing the force by two as the water will only flow underneath the screen. This is illustrated in Figure 5.16 below.

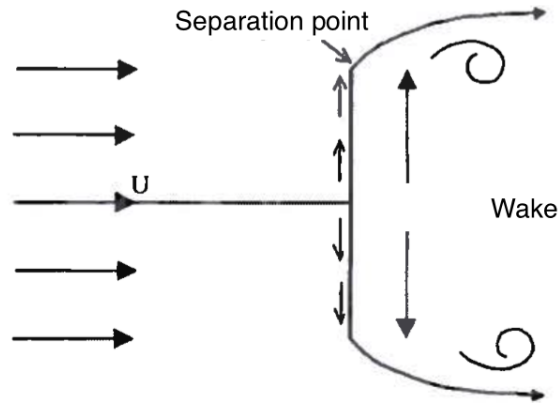


Figure 5.16: Streamlines past a flat plate (Pettersen, 2007).

The drag coefficient of a flat plate in a uniform stream is 1.98 (Hoerner, 1985). The total drag force acting on the screen is further calculated by the following drag equation:

$$D_{sys} = \frac{1}{2} \rho V_{sys}^2 C_D \cdot (2l) \cdot b \quad (5.17)$$

where V_{sys} is the total speed of the system and $2l$ is two times the depth of the screen (6 m).

5.6.3 Total thrust

As System 001 is assumed to drift at the same speed as the surface particles, the relative speed between the system and the water is zero. However, as the foil generates thrust, the system will move faster than the water, creating drag in the opposite direction and slow down the system. The increase in velocity of the system is thus a result of the thrust produced by the foil minus the drag force of the system. The total velocity of the system can be calculated by using Equation 5.17 above, where V_{sys} is the total speed of the system. Thus, the state of equilibrium will be achieved when the following equation is fulfilled:

$$\frac{1}{2} \cdot D_{sys} = T \quad (5.18)$$

From this, V_{sys} can be calculated.

Chapter 6

Results

This chapter contains the relevant results obtained from the modelling described in Chapter 5. The model is, as mentioned previously, based on multiple assumptions. In this chapter, additional assumptions related to calculations are presented where relevant. Further, the thrust obtained by using passive oscillating foils for additional propulsion on the system will be presented. An estimation of the total additional speed of the system, including the floater and screen will also be presented. Finally, the results will be discussed and compared in order to determine whether the results obtained are reasonable or if too many assumptions have been made to determine the feasibility of the concept.

6.1 Wave characteristics

The weather data obtained in Chapter 3 was used as a basis for the calculations in this thesis. In addition, the wavelength, λ , wave number, k , phase velocity, c_w and wave frequency, ω , were calculated by using formulas presented in Section 5.1.1. These values were further used to calculate the net horizontal drift velocity of the surface particles, U . Table 6.1 contains the wave characteristics of the model used in this thesis.

Table 6.1: Wave characteristics.

| | | Units |
|--------------------------------|-----------------|----------------|
| Peak wave period, T_p | 3.9872 | s |
| Significant wave height, H_s | 0.8586 | m |
| Wavelength, λ | 24.8213 | m |
| Wave number, k | 0.2531 | $1/m$ |
| Phase velocity, c_w | 6.2253 | m/s |
| Wave frequency, ω | 1.5758 | $1/s$ |
| Stokes net drift velocity, U | 0.0735 (0.1429) | m/s (kn) |

6.1.1 Heave motion, velocity and acceleration

As the foil is placed at a depth of $\lambda/2 = 12\text{ m}$, the particle motions are assumed negligible. Thus, the motions of the foil are dependent on the induced heave and pitch motion. As the values change at every time instant, a table with values from six different time instants during one period, T_s , is presented. These points are marked in Figure 6.1 below from A-F. The heave motion, $h(t)$, heave velocity, $\dot{h}(t)$, and heave acceleration, $\ddot{h}(t)$, of the foil are presented in Table 6.2 below.

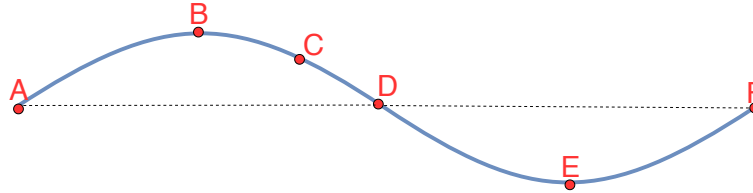


Figure 6.1: Reference points A-F during one wave period.

Table 6.2: Heave motion, velocity and acceleration.

| Point | t [s] | $h(t)$ [m] | $\dot{h}(t)$ [m/s] | $\ddot{h}(t)$ [m/s ²] |
|-------|---------------------|------------|--------------------|-----------------------------------|
| A | 0 | 0 | 0.6765 | 0 |
| B | 0.9968 ($T_p/4$) | 0.4293 | 0 | -1.0661 |
| C | 1.4952 ($3T_p/8$) | 0.3036 | -0.4784 | -0.7538 |
| D | 1.9936 ($T_p/2$) | 0 | -0.6765 | 0 |
| E | 2.9904 ($3T_p/4$) | -0.4293 | 0 | 1.0661 |
| F | 3.9872 (T_p) | 0 | 0.6765 | 0 |

6.1.2 Effective inflow velocity, $V(t)$

From quasi-static theory, the effective inflow velocity can be found by use of Equation 5.4. The inflow velocity is thus a function of the horizontal drift velocity and the vertical heave velocity. Figure 6.2 below illustrates the effective inflow velocity as a function of time. The blue arrows indicate the angle at which the inflow velocity is acting on the foil. As seen in the figure, the inflow velocity is approximately $\phi = 90^\circ$ on the foil during the heave motion, while where there is no heave motion, the horizontal velocity is dominant.

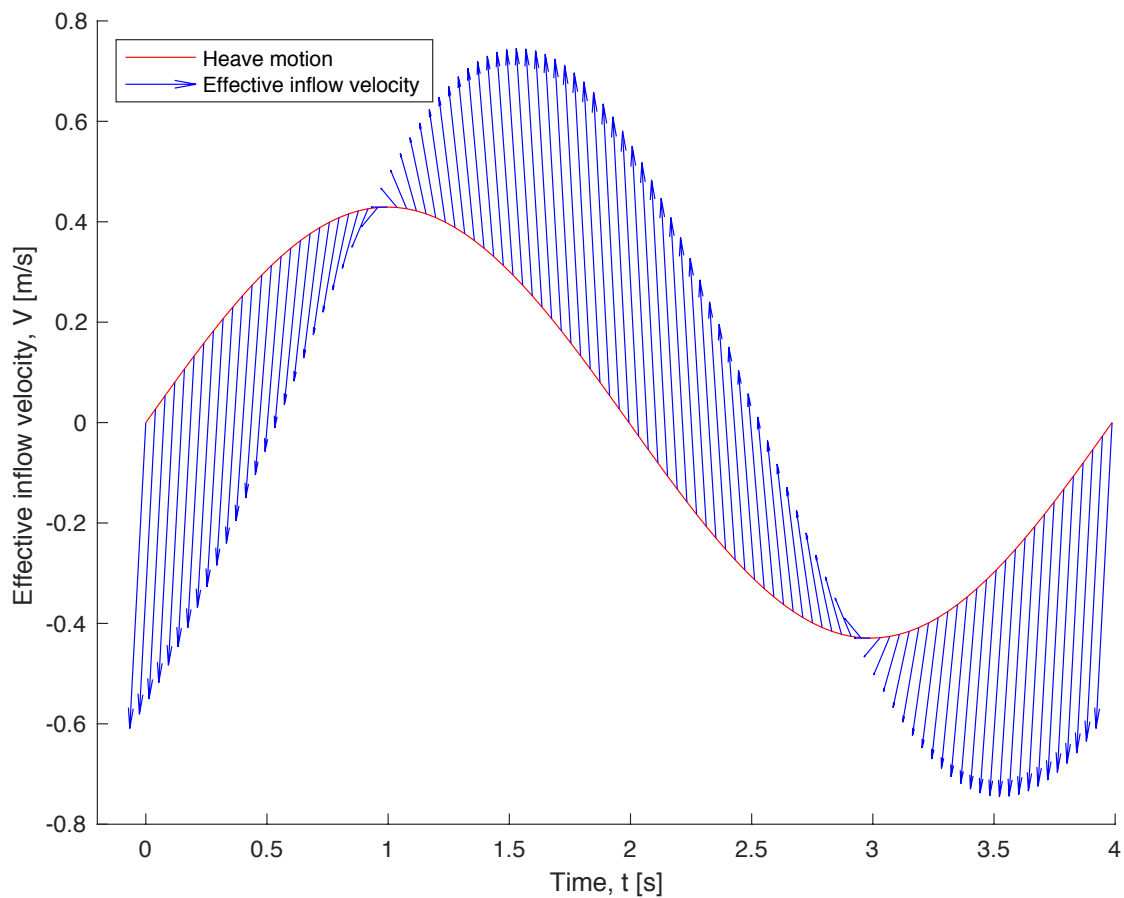


Figure 6.2: Effective inflow velocity, $V(t)$. The blue arrows indicate the angle at which the effective inflow velocity is acting on the foil.

6.2 Foil characteristics

The foil used in this thesis is a NACA 0012 profile. The length of the chord and span were chosen for the purpose of estimating thrust and have not been optimised. Based on literature and previous research, the added mass point of action was set to half-chord, while the lift and drag force point of action was originally set to quarter-chord. However, as the foil will be operating with angles of attack above stall, the foil starts to act like a plate, moving the center of force closer to half-chord. Table 6.3 below represents the foil characteristics in this model.

Table 6.3: Foil dimensions.

| | | Unit |
|--------------------------------------|-------|-------|
| Chord, c | 1 | m |
| Span, b | 2 | m |
| Camber | 0 | % |
| Area, S | 2 | m^2 |
| Center of added mass force, x_a | $c/2$ | m |
| Center of lift and drag force, x_f | $c/2$ | m |

6.3 Forces acting on foil

Calculating the drag and lift forces acting on the foil by use of quasi-static theory requires drag and lift coefficients, C_D and C_L . Non-dimensional coefficients are expressed as the ratio between actual force and kinetic force in the undistributed flow-field and are dependent on the Reynolds number. The kinematic viscosity of sea water is set to $1.18 \cdot 10^{-6} \text{ m}^2/\text{s}$.

$$R_N = \frac{U \cdot c}{\nu} = 62,288 \quad (6.1)$$

6.3.1 Experimental lift and drag coefficients, C_L and C_D

Experimental data was extracted from experiments conducted with Reynolds number $R_N = 80,000$. The tabulated data can be found in Appendix B.1. Figure 6.3 below illustrates the lift and drag coefficients for a NACA 0012 foil at $R_N = 80,000$. As seen in the figure, the lift coefficient twice reaches a local maximum before decreasing, while the drag coefficient increases until the angle of attack is 90° . From the second maximum at 45° , the lift coefficient starts decreasing again, leaving the curve of the lift coefficient behaving much like a bell curve.

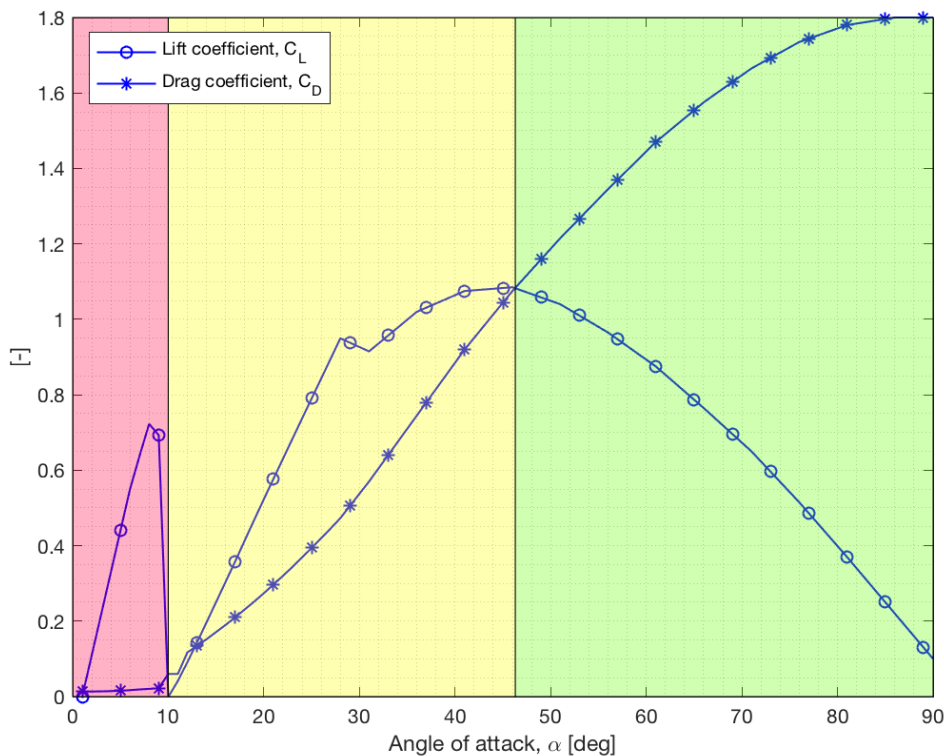


Figure 6.3: Lift and drag coefficients for a NACA 0012 foil at $R_N = 80,000$.

Above stall angles, most foils behave like a flat plate. According to this experimental data, the foil will stall if the angle of attack is increased above 8° . The lift coefficient starts increasing as the angle of attack moves beyond 10° and will reach its second maximum at $\alpha \approx 45^\circ$ with a value close to $C_L = 1.1$. When $\alpha = 90^\circ$ the lift coefficient is approximately 0.1 and the drag coefficient is 1.8, which is similar to that of a flat plate ($C_D \approx 1.95$). This is due to the flow separating and an increase in the thickness of the boundary layer, which results in the shape having little or no effect on its stalled region (Hoerner, 1985).

Keeping in mind that the angle of attack is defined as in Figure 5.7, the angle of attack is zero when the foil is vertical and 90° when the foil is horizontal. In real life, it would be desirable to require a spring stiffness that avoids the angles of attack from 0° to the stalling angle, i.e. the red region in the figure. In addition, a foil operating in the green region of the foil, i.e. with angles of attack between 45° and 90° , is desirable as the lift coefficient decreases if the foil pitches enough to operate in the yellow region in the figure, i.e. between 10° and 45° . In general, it will be desirable to operate in the region where the lift force is larger than the drag force. However, as the inflow is vertical on the foil, the drag will contribute to the vertical movement of the foil, which is essential in order for the foil to pitch sufficiently. As the drag is related to the water that is displaced by the foil when it moves up and down with the heave motion.

6.3.2 Added mass

The added mass, which is a function of the projected area of the foil, varies with change in angle of attack and is calculated by use of Equation 5.11. Table 6.4 below represents the added mass at different angles of attack.

Table 6.4: Added mass on hydrofoil.

| Angle of attack, α [deg] | Added mass, m_A [kg] |
|---------------------------------|------------------------|
| 1 | 0.49 |
| 10 | 48.55 |
| 30 | 402.52 |
| 45 | 805.03 |
| 60 | 1207.55 |
| 80 | 1561.52 |
| 90 | 1610.07 |

6.4 State of equilibrium

A pitching moment will at each instant in time be imposed on the foil. Finding the optimal spring stiffness and distance between the point where the lift and drag forces are acting, $x_a = c/2$, and the pivot point, x_p , requires a comprehensive iteration process. Both the spring stiffness and the pivot point should be chosen such that the foil will be in moment equilibrium at every time step. In other words, the equilibrium equation referred to as Equation 5.14 must be fulfilled at every time step.

For a fixed spring stiffness and pivot point, the iteration process thus becomes an optimisation model of pitching angle. The model finds the pitching angle at which there is a moment equilibrium for every time step. In cases where there are multiple solutions, the model will choose the pitch angle that gives the highest thrust force.

6.4.1 Pivot point, x_p , and spring stiffness, k_s

In order for the foil to pitch in the right direction, the pivot point of the foil should be placed somewhere between $x = c/2$ and $x = c$ as illustrated in Figure 5.12. The distance is measured from half-chord towards the leading edge (LE). It was desirable to optimise the position of the pivot point by comparing thrust generated by use of different pivot point positions.

The foil must be installed with a spring to counteract the hydrodynamic moment created by the force acting on the foil (Zhu, 2012). However, if the spring stiffness is too high, the foil will not be able to pitch sufficiently and thus will not produce sufficient thrust. As the spring stiffness reduces, the foil will be able to reach higher pitch angles, resulting in more thrust. Figure 6.4 below illustrates the relationship between pivot point position, spring stiffness, and thrust generated in waves with a wave period of 3.9872 s .

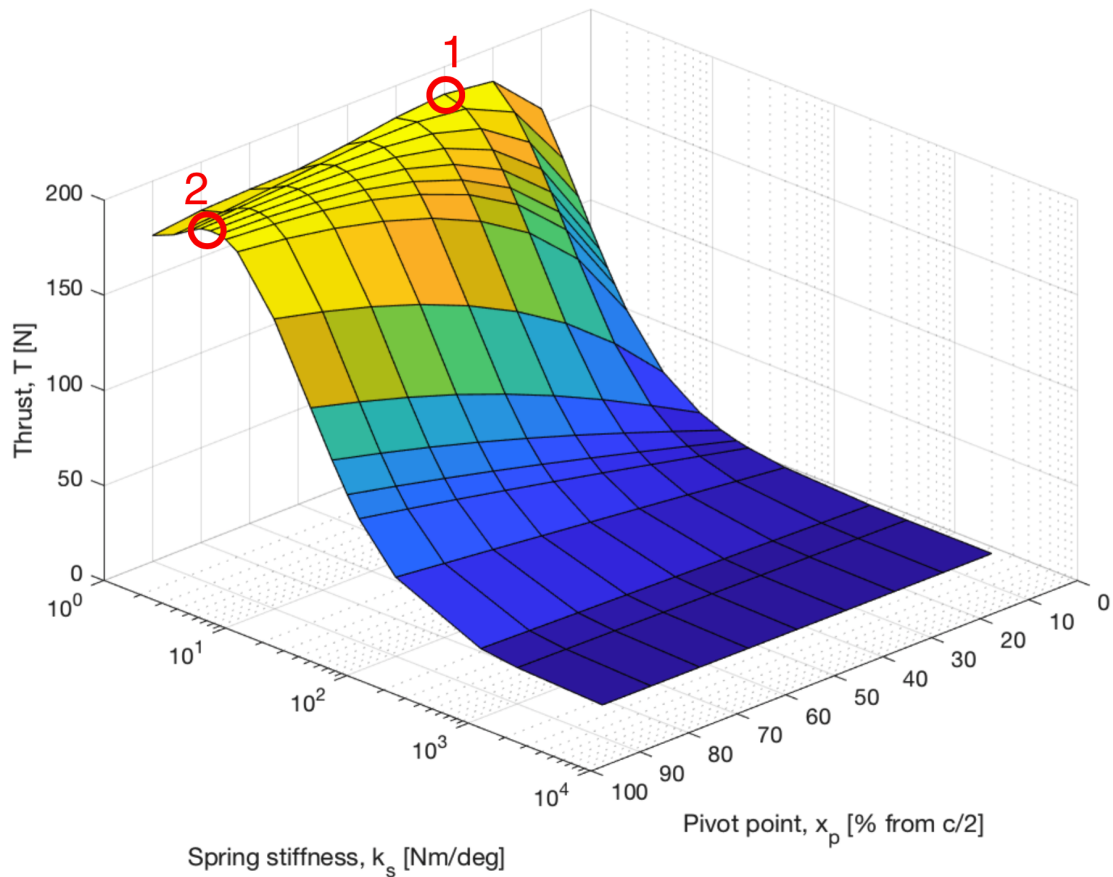


Figure 6.4: Relationship between pivot point, spring stiffness and thrust produced. 1: $k_s = 1 \text{ Nm/deg}$, $x_p = 0.15 \text{ m}$. 2: $k_s = 3 \text{ Nm/deg}$, $x_p = 0.45 \text{ m}$. x_p is measured from half-chord towards LE.

As seen in the figure above, the use of springs of too high stiffness, e.g. $> 10^2 \text{ Nm/deg}$, results in little to no thrust. However, as the spring stiffness is reduced, more thrust is produced. Placing the pivot point closer to the leading edge will give a larger moment about the pivot point as the distance to the center of force is larger. Another observation made from looking at the figure is that the highest thrust production occurs a spring stiffness in the range of 1-3 Nm/deg is chosen. This results in a thrust production close to 200 N .

By choosing a spring stiffness of 1 Nm/deg , the maximum thrust occurs with a pivot point placed 0.15 m from the half-chord point, while if a spring stiffness of 3 Nm/deg is chosen, the optimal pivot point position is found to be 0.45 m from the half-chord point.

Comparing these values with values obtained in other sea states, with longer wave periods, shows a significant difference in required spring stiffness to obtain the same amount of thrust. By increasing the wave period, the thrust is reduced for the same spring stiffness. However, as the wave height is increased, so is the thrust obtained by the hydrofoils.

Using the maximum values from the weather data obtained in Chapter 3, significantly more thrust would be generated. In addition, by placing the pivot point closer to the leading edge, the spring stiffness required would be significantly higher under these weather conditions than the spring stiffness required under calm weather conditions with the same pivot point. Nevertheless, by placing the pivot point closer to the center of the foil, a lower spring stiffness, close to the one required under calm conditions, would be necessary. This indicates that placing the pivot point relatively close to the center of the foil would provide desirable thrust under several sea conditions. The spring stiffness was found by use of the MATLAB scripts *foil_thrust.m* and *spring_pivot_plot.m* in Appendix A.2 and A.3, respectively.

6.4.2 Angles

The angles at each time instant are found through the iteration process. Using the inflow velocity angle as a starting point, the angle of attack increased as the pitch angle decreases.

Angle of attack, α

The instantaneous angle of attack, $\alpha(t)$, depends on both the heave and the pitch motion of the foil. The angle of attack could be calculated by finding the inflow angle at every time instant and calculating the pitch angle from Equation 5.8 (Yulin Pan, n.d.). This would make it possible to include the phase difference between the heave and pitch motion. The angle of attack is found through an iteration process to find the optimal value when both the spring stiffness, k_s , and the pivot point, x_p , are non-variable. A phase angle of $\psi = 90^\circ$ and vertical effective inflow would result in the following plot.

Pitch angle, θ

The pitch angle is calculated from the state of moment equilibrium in Equation 5.14. These angles are associated with the maximum lift force produced at each time instant. The plot in Figure 6.5 shows the resulting pitching from fixing the spring stiffness.

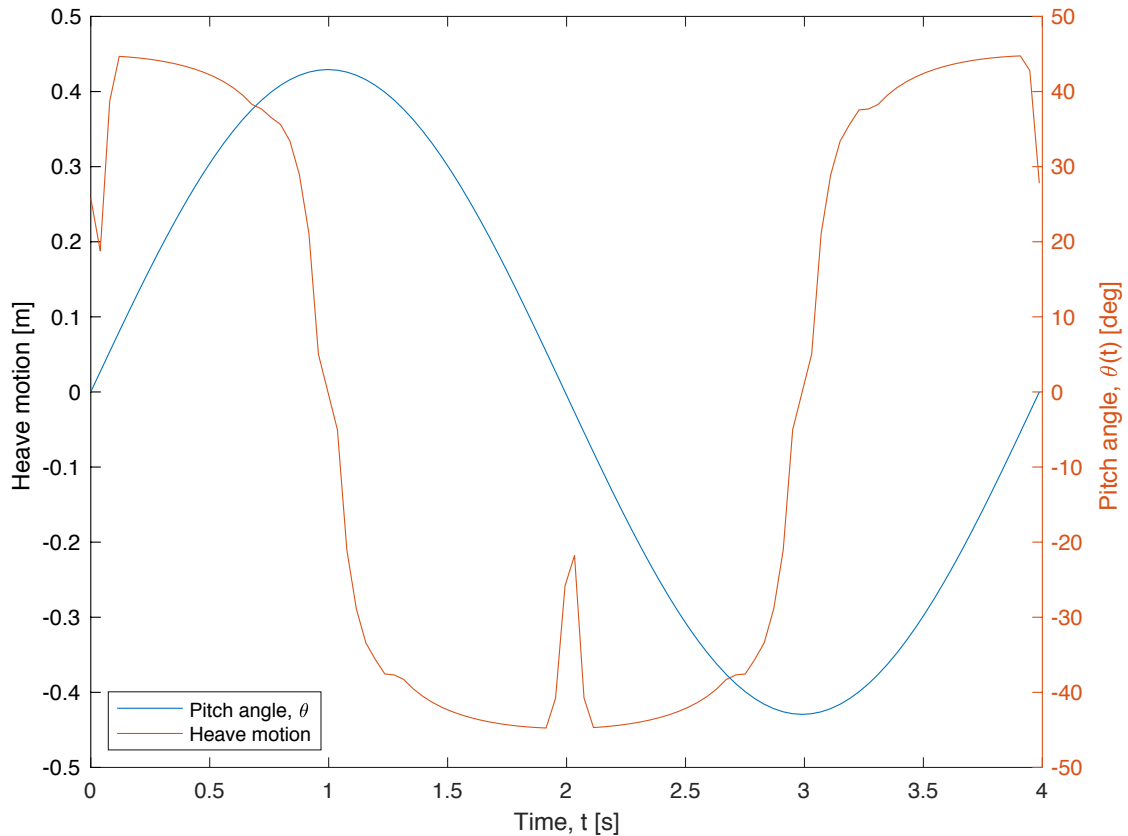


Figure 6.5: Pitch angles for fixed spring stiffness.

As seen of the figure above, the pitch angle moves between approximately 45° and -45° with a phase difference close to 90° . As seen in the figure, the pitch angle at $t = 0$, $t = T_p/2$ and $t = T_p$ have some abnormalities. This may be due to the fact that the MATLAB script takes into account the effect of the horizontal drift flow, which alters the inflow angle at every instant in time. If the pitching angle reaches the same angle as the inflow angle, the result is zero angle of attack. Further, a zero angle of attack leads to an added mass force of zero. This results in a significant decrease in the hydrodynamic moment, which requires a lower pitch angle to obtain moment equilibrium with a fixed spring stiffness and pivot point.

6.5 Calculating thrust

By using quasi-static angles of attack and finding the corresponding lift coefficients through experimental data available, the instantaneous thrust can be calculated. The average thrust can further be calculated from the thrust obtained at each time-step (Ahmed, Welaya, & Abdulmotaleb, 2017). Equation 6.2 below calculates the mean thrust by use of quasi-static theory.

$$\bar{T}_{foil,qs} = \frac{\sum T_{ins}}{\text{Number of time steps}} \quad (6.2)$$

where T_{ins} is the instantaneous thrust at each time step. Figure 6.6 below is a plot of the lift force on the foil with fixed spring stiffness. This resulted in an average thrust of 116 N.

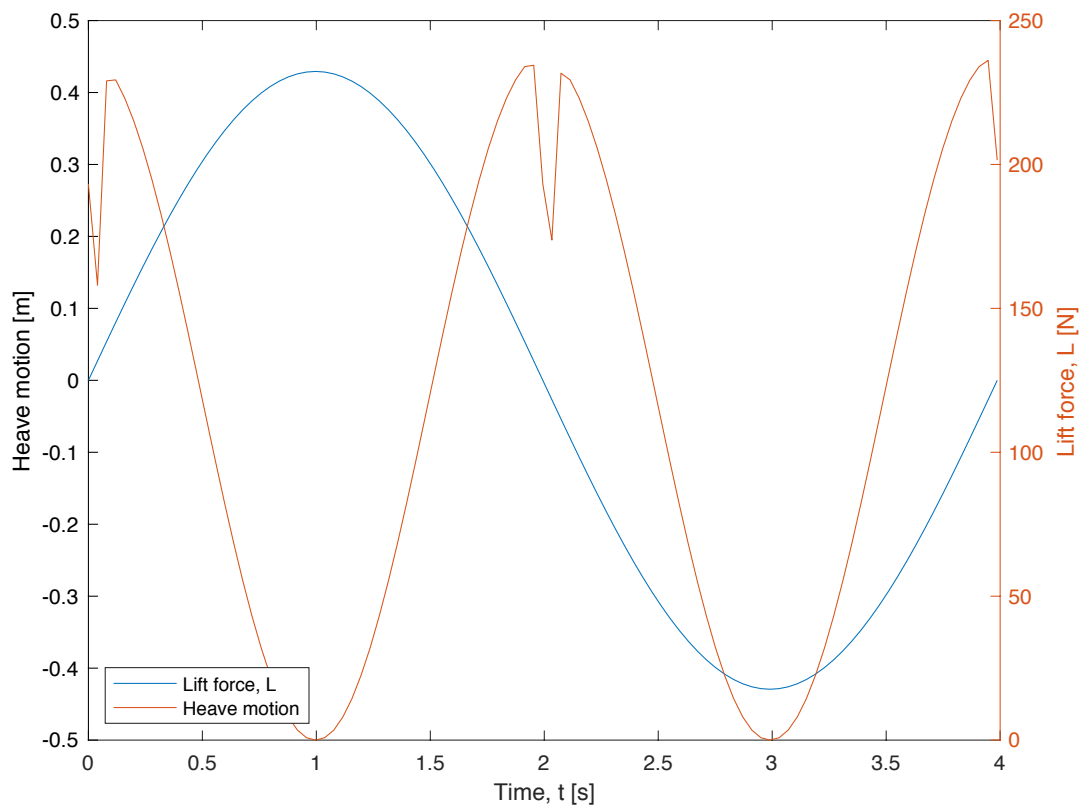


Figure 6.6: Lift force acting on the foil with fixed spring stiffness.

The plot above shows the same tendencies as the plot in Figure 6.5 at $t = 0$, $t = T_p/2$ and $t = T_p$, and can be explained in the same way. This will have an impact on the average thrust of the system as the lift is registered lower than it should be at these three points. However, as these calculations are based upon multiple assumptions, it is reasonable to assume that this will not be the decisive factor determining whether this is a feasible concept or not. As seen in the figure, the maximum lift occurs at the maximum pitch angle, i.e. at the maximum steepness of the wave.

According to a study by Duarte (2011), a pitching foil was tested in waves with a wave height of 0.1 m . The experiment showed that multiple springs with a stiffness of 5.329 Nm/deg resulted in the best propulsion (Duarte, 2011). This indicates that a spring stiffness in the range $1\text{-}3\text{ Nm/deg}$, which has been tested in this thesis, is reasonable for generating maximum thrust for a foil with a chord length of 1 m and a span of 2 m .

6.5.1 Forces on System 001

Previously in this thesis, it has been assumed that System 001, without the use of foils, will drift at the same speed as the mean vertical particle velocity on the surface, i.e. $U = 0.0735\text{ m/s}$. This will however most likely not be the case as the system will also be affected by other forces, such as wind. Nevertheless, the focus of this study is to look at the effect of the additional thrust obtained by the use of passive oscillating foils. As the foil generates thrust forward, a drag force will be induced on the system in the opposite direction.

The calculations performed in this thesis do not take into account the deformation of the screen as it is assumed to be rigid enough to withstand significant deformation. Assuming that the screen drifts at the same speed as the horizontal net drift velocity, the additional thrust provided by the use of foils will lead to a drag force acting in the opposite direction. Using Equation 5.17, the total increase in velocity is calculated as follows:

$$V_{sys} = \sqrt{\frac{\frac{1}{2} \cdot 116 \cdot 2}{\frac{1}{2} \cdot 1025 \cdot 1.98 \cdot (2 \cdot 3)}} = 0.1952\text{ m/s} \quad (6.3)$$

This is calculated as the total increase in speed due to the use of passive oscillating foils per m of the system. In order to calculate the total increase of velocity for the whole system, it would be relevant to determine how many foils to use and the orientation of the foils.

Chapter 7

Discussion

7.1 Concept choice

The concept that was chosen to research further in this thesis was related to the utilisation of the energy of waves to generate thrust. The model showed that it was possible to generate additional propulsion in calm conditions by using passive oscillating foils. However, this concept was not compared with other concepts utilising the same sets of natural forces under the same conditions. This could have indicated whether the concept researched in this thesis was the best choice when looking at the optimisation of wave exploitation under calm conditions.

Comparing a concept that utilises the waves in the area with a concept that utilises the wind or currents would have given insight into whether waves are the most efficient natural force to use. This could be done by looking deeper into the use of rudders, sails or other concepts that focus on the utilisation of other forces. Comparing these results to the results obtained by use of passive oscillating foils would have given an indication as to whether it would be more beneficial to utilise other natural forces in the area.

Lastly, the concepts discussed in this thesis are based on the weather data available for the area of interest. However, as the information about the drifting pattern of the system was not available, the minimum values were used as a basis for the concept development phase. Nevertheless, the system may not operate within these conditions often and the system may thus be designed for unreasonable conditions. The system might experience the same retention problem in weather conditions that are characterised as "less calm", i.e. higher waves.

7.2 Model design

It was desirable to create a model with three variables. These were the position of the pivot point, x_p , spring stiffness, k_s and pitch angle, θ . As the aim of using a model was to find an estimate to determine if the use of passive oscillating foils could produce additional thrust on the system, simplifications were made. These simplifications were mainly related to the forces acting on the system and would have to be re-evaluated if more precise calculations were to be done.

In real life, the screen will not be vertically placed under the pipe when a wave passes. The motion of the screen will depend on the degree of freedom of both the screen and the pipe. For the purpose of this thesis, the system was assumed to move vertically up and down with the waves. This will have an effect on the calculations as the drag force acting on the system is dependent on the frontal area of the system, and the angle between the screen and the inflow velocity.

In addition, as the model design turned out to be more comprehensive than anticipated, the calculations in this report were conducted for one foil with one spring. This gives an estimate for the thrust that can be generated by use of passive oscillating foils. For the calculations of total thrust obtained by the system with passive oscillating foils, a simplified model of the floater and screen was taken into consideration. This may have a significant effect on the total thrust of the system and is very relevant for the determination of feasibility.

The model was setup based on quasi-static theory and used empirical data obtained from experiments. This theory describes unsteady flow by steady-state principles, which may be a blunt assumption. As the foil is subjected to an instantaneous change in angle of attack, the lift is calculated by instantaneous step-functioned angles. In real life, the foil may not have the same angle of attack long enough for a steady-state flow and circulation to arise. It would therefore have been more accurate to use unsteady theory. However, this was beyond the scope of this thesis.

Chapter 8

Conclusion

This thesis has investigated the use of passive oscillating foils for additional propulsion. A model of the concept, which was identified during the concept development phase of this thesis, was created based on multiple assumptions. The model was used to determine the feasibility of this concept under calm conditions, as this is where the retention problem arises. As this thesis looks at worst case scenarios, i.e. calm weather periods with relatively small waves and wind speeds, the results may be conservative.

The total thrust obtained by the use of passive oscillating foils was estimated to be 116 N for a NACA 0012 profile of chord length $c = 1\text{ m}$ and span $b = 2\text{ m}$. Further, the total increase in speed was calculated to be 0.1952 m/s . As the system is assumed to drift at a speed of 0.0735 m/s prior to the installation of foils, the results indicate that the system may be able to increase its speed by 165% under the given conditions. Thus, the results obtained in this thesis indicate that the system may be able to move faster than the plastic by use of passive oscillating foils.

It is however important to keep in mind that the results are based on multiple assumptions and would have to be calculated more carefully before the concept can be applied to the system.

Chapter 9

Further work

Although the concept researched in this thesis is found to be a feasible solution, based on the assumptions made, it will still be relevant to assess other solutions to the retention problem. This includes other methods for increasing the speed of the system, as well as looking at methods for slowing the system enough to reverse the process. Further, it would be relevant to look at other concepts utilising waves, such as wave gliders. Another line of investigation would be to compare the concept of passive oscillating foils with concepts that utilise other forces, such as wind and currents. This would give an indication as to whether the use of passive oscillating foils is the best option.

In order to optimise the model design of the concept discussed in this thesis, the next scope of work should be to investigate an optimisation of number of foils and orientation of these foils. In addition, it would be relevant to look at different foil profiles and compare results to find the optimal choice. The span, chord length and thickness of the foil may have a significant affect on the final results. The estimation of forces acting on the floater and screen are simplified and may have a significant affect on the final results. It would therefore be desirable to create a more complex model that takes the whole system into account.

The hydrodynamic calculations conducted in this thesis are based on quasi-static theory with empirical data. In order to calculate the response of the system with hydrofoils more accurately than in this thesis, the unsteady lift formula introduced by Theodorsen can be utilised. This is written about by T. Ahmed, Y Welaya and S. Abdulmotaleb in a report titled *Numerical Modeling of the Hydrodynamic Performance of Hydrofoils for Auxiliary Propulsion of Ships in Regular Head-Waves* and will be valuable if this model was to be optimised hydrodynamically (Ahmed et al., 2017).

It would also be recommended to look at the possibilities of performing a CFD analysis to calculate the total forces acting on the system, as this will provide more accurate results. If possible, conducting experimental test would also be beneficial in order to gain a better understanding of the response of the system when passive oscillating foils are implemented.

References

- ABM Yacht Support. (2017). *Are we doing all what we can to keep clean oceans?* Retrieved 31 January 2019, from <http://www.abmyachtsupport.com/2017/09/can-keep-clean-oceans/>
- Ahmed, T., Welaya, Y., & Abdulmotaleb, S. (2017). Numerical modeling of the hydrodynamic performance of hydrofoils for auxiliary propulsion of ships in regular head-waves.. doi: 10.1115/OMAE2017-61333
- Amdahl, J., Berge, S., Dukan, F., Endal, A., Hals, J., Holm, H., ... Æsøy, V. (2014). *Havromsteknologi : et hav av muligheter*. Bergen: Fagbokforlaget.
- AUVAC. (n.d.). *AUV System Spec Sheet*. Retrieved from <https://auvac.org/platforms/view/259>
- Bigg, G. R. (2003). *The oceans and climate* (2nd ed.). Cambridge: Cambridge University Press.
- Britannica Academic. (2017). *Beaufort scale*. Retrieved 21 March 2019, from <https://academic.eb.com/levels/collegiate/article/Beaufort-scale/13985>
- Chen, J., Ge, Y., Yao, C., & Zheng, B. (2018). Dynamics modeling of a wave glider with optimal wing structure. *IEEE Access*, 6, 71555–71565.
- Colling, A., Brown, E., & Open University Oceanography Course Team. (2001). *Ocean circulation* (2nd ed., Vol. 3). Oxford: Butterworth Heinemann in association with the Open University.
- Corones, M. (2015). *How aerodynamic stall occurs*. Retrieved 21 March 2019, from <http://blogs.reuters.com/data-dive/2015/01/07/how-aerodynamic-stall-occurs/>
- Dagestad, I. (2018). *Actuation moments for hydrofoil flaps*. NTNU. Retrieved from <http://hdl.handle.net/11250/2564516>
- DNV GL. (2017). *DNVGL-RP-C205. Environmental conditions and environmental loads*. Det Norske Veritas. Retrieved from <http://rules.dnvgl.com/docs/pdf/DNV/codes/docs/2017-08/RP-C205.pdf>
- Duarte, T. M. (2011). *Experimental study of a 2d hydrofoil for application in ocean mooring systems*. 9th EWTEC Conference in Southampton, England.
- Eitzen, F. C. (2012). *Mathematical modelling of a foil propulsion system*. Institutt for marin teknikk. Retrieved from <http://hdl.handle.net/11250/238215>

REFERENCES

- GeoGarage. (2018). *Ocean cleanup : A 600-meter-long plastic catcher heads to sea, but scientists are skeptical*. Retrieved from <http://blog.geogarage.com/2018/09/ocean-cleanup-600-meter-long-plastic.html>
- Gray, A. (2018). *90% of plastic polluting our oceans comes from just 10 rivers*. Retrieved from <https://www.weforum.org/agenda/2018/06/90-of-plastic-polluting-our-oceans-comes-from-just-10-rivers/>
- Gregory, M. R. (2009). *Environmental implications of plastic debris in marine settings - entanglement, ingestion, smothering, hangers-on, hitch-hiking and alien invasion* (Vol. 364) (No. 1526).
- Hanley, S. (2016). *Dolphin tail more efficient than propeller for ships*. Retrieved from <https://gas2.org/2016/12/29/dolphin-tail-more-efficient-propeller-ships/>
- Hauge, J. (2013). *Oscillating foil propulsion*. Institutt for marin teknikk. Retrieved from <http://hdl.handle.net/11250/238732>
- Henry, D. (2019). Stokes drift in equatorial water waves, and wave-current interactions. *Deep-Sea Research Part II*, 160, 41–47.
- Hoerner, S. F. (1985). *Fluid-dynamic lift : practical information on aerodynamic and hydrodynamic lift* (2nd ed. ed.). Brick Town, N.J.: Liselotte A. Hoerner.
- Howell, E. A., Bograd, S. J., Morishige, C., Seki, M. P., & Polovina, J. J. (2012). On north pacific circulation and associated marine debris concentration. *Marine Pollution Bulletin*, 65(1), 16–22. Retrieved from <http://www.sciencedirect.com/science/article/pii/S0025326X11002372> (At-sea Detection of Derelict Fishing Gear) doi: <https://doi.org/10.1016/j.marpolbul.2011.04.034>
- Krogstad, H. E., & Arntsen, A. (2000). *Linear wave theory part a - regular waves*. NTNU.
- Latitude. (2018). *Satellite map of great pacific garbage patch*. Retrieved 9 February 2019, from <https://latitude.to/satellite-map/general/337/great-pacific-garbage-patch>
- Lebreton, L., Slat, B., Ferrari, F., Sainte-Rose, B., Aitken, J., Marthouse, R., ... Reisser, J. (2018). Evidence that the great pacific garbage patch is rapidly accumulating plastic. *Sci Rep*, 8(1), 4666–4666.
- Li, X.-t., Liu, F., Wang, L., & She, H.-q. (2017). Motion analysis of wave glider based on multibody dynamic theory. In Y. Huang, H. Wu, H. Liu, & Z. Yin (Eds.), *Intelligent robotics and applications* (pp. 721–734). Cham: Springer International Publishing.
- Liu, Y. (2013). Establishment of a wave energy and technology lab to promote the experimental study of ocean and wave energy. In (Vol. 6, pp. 1–8). doi: 10.1115/IMECE2013-62968
- Manley, J., & Willcox, S. (2010). The wave glider: A new concept for deploying ocean instrumentation. *IEEE Instrumentation Measurement Magazine*, 13(6), 8–13.
- Mannam, P., Krishnankutty, P., & Mallikarjuna, J. (2014). Experimental

REFERENCES

- study of flapping foil propulsion system for ships and underwater vehicles and piv study of caudal fin propulsors. In (pp. 1–7). doi: 10.1109/AUV.2014.7054404
- Myrhaug, D. (2006). *Oceanography: wind, waves* (Vol. UK-2006-78). Trondheim: Marinteknisk senter, Institutt for marin teknikk.
- Pettersen, B. (2007). *Marin teknikk 3 : hydrodynamikk*. Trondheim: Marinteknisk senter, Institutt for marin teknikk.
- Read, D., Hover, F., & Triantafyllou, M. (2003). Forces on oscillating foils for propulsion and maneuvering. *Journal of Fluids and Structures*, 17(1), 163–183.
- Riley, E. F. (2015). *The potential energy savings by application of a wave foil on the autonomous container vessel revolt*. NTNU. Retrieved from <http://hdl.handle.net/11250/2350718>
- Rochman, C. (2016). Strategies for reducing ocean plastic debris should be diverse and guided by science. *Environmental Research Letters*, 11(4).
- Schouveiler, L., Hover, F., & Triantafyllou, M. (2005). Performance of flapping foil propulsion. *Journal of Fluids and Structures*, 20(7), 949–959.
- Sheldahl, R. S., & Klimas, P. C. (1981). *Aerodynamic characteristics of seven symmetrical airfoil sections through 180-degree angle of attack for use in aerodynamic analysis of vertical axis wind turbines*. Sandia National Laboratories. Retrieved from <https://www.osti.gov/servlets/purl/6548367/>
- Sherman, P., & van Sebille, E. (2016). Modeling marine surface microplastic transport to assess optimal removal locations. *Environmental Research Letters*, 11(1). Retrieved from <http://search.proquest.com/docview/1776646104/>
- Simpson, B., Licht, S., Hover, F., & Triantafyllou, M. (2008). Energy extraction through flapping foils. In *Proceedings of the international conference on offshore mechanics and arctic engineering - omae* (Vol. 6, pp. 389–395).
- Slat, B. (2018). *The final design of the world's first cleanup system*. Retrieved from <https://www.theoceancleanup.com/updates/the-final-design-of-the-worlds-first-cleanup-system/>
- Slat, B., Ardiyanti, A., Arens, E., Bolle, E., Brugman, H., Campbell, H., ... de Sonnevile, J. (2014). *Feasibility study - the ocean cleanup*. The Ocean Cleanup.
- Steen, S. (2011). *Motstand og propulsjon, propell- og foilteori* (Vol. UK-2011-99). Trondheim: Marinteknisk senter, Institutt for marin teknikk.
- Sverdrup, K. A. (2008). *An introduction to the world's oceans* (9th ed.). Boston: McGraw-Hill Higher Education.
- Thawewat, N., Phoemsapthawee, S., & Juntasaro, V. (2018). Semi-active flapping foil for marine propulsion. *Ocean Engineering*, 147, 556–564.
- The Ocean Cleanup. (n.d.-a). *Our solution*. Retrieved 23 January 2019, from <https://www.theoceancleanup.com>
- The Ocean Cleanup. (n.d.-b). *System 001*. Retrieved 23 January 2019, from

REFERENCES

- <https://www.theoceancleanup.com/system001/>
- The Ocean Cleanup. (n.d.-c). *Technology - how it works*. Retrieved 23 January 2019, from <https://www.theoceancleanup.com/technology/>
- The Ocean Cleanup. (n.d.-d). *Wilson update - tweaking the system*. Retrieved 23 January 2019, from <https://www.theoceancleanup.com/updates/wilson-update-tweaking-the-system/>
- The Ocean Cleanup. (2018a). *Testing continues to understand system behaviour*. Retrieved 23 January 2019, from <https://www.theoceancleanup.com/updates/testing-continues-to-understand-system-behavior/>
- The Ocean Cleanup. (2018b). *Testing continues to understand system behaviour*. Retrieved 24 January 2019, from <https://www.theoceancleanup.com/updates/testing-continues-to-understand-system-behavior/>
- The Ocean Cleanup. (2019). *System design upgrades completed, to be relaunched in june*. Retrieved 25 May 2019, from <https://www.theoceancleanup.com/updates/system-design-upgrades-completed-to-be-relaunched-in-june/>
- UNEP. (2014). *Valuing plastic: The business case for measuring, managing and disclosing plastic use in the consumer goods industry*.
- White, F. M. (2011). *Fluid mechanics* (7th ed. ed.). New York: McGraw-Hill.
- Willis, J. (2013). Wake sorting, selective predation and biogenic mixing: potential reasons for high turbulence in fish schools. *Peerj*, 1(1).
- World Economic Forum. (2016). *The new plastics economy: Rethinking the future of plastics*. Retrieved from http://www3.weforum.org/docs/WEF_The_New_Plastics_Economy.pdf
- Xiao, Q., & Zhu, Q. (2014). A review on flow energy harvesters based on flapping foils. *Journal of Fluids and Structures*, 46(C), 174–191.
- Yang, F., Shi, W., Zhou, X., Guo, B., & Wang, D. (2018). Numerical investigation of a wave glider in head seas. *Ocean Engineering*, 164, 127–138.
- Yttervik, R. (2004). *Ocean current variability in relation to offshore engineering* (Vol. 151). Trondheim: Norwegian University of Science and Technology, Faculty of Engineering Science and Technology, Department of Marine Technology.
- Yulin Pan. (n.d.). *VFRL selected research areas*. Retrieved 6 February 2019, from <http://web.mit.edu/vfrl/www/research/Yulin.html>
- Zhu, Q. (2012). Energy harvesting by a purely passive flapping foil from shear flows. *Journal of Fluids and Structures*, 34, 157–169.

A MATLAB-script

A.1 weather_data.m

```
1 clear all;
2 clc;
3 close all;
4
5 %use ncdisp to see your file
6
7 lat=double(ncread('downloadny2018.nc','latitude')); %
   latitude coordinate
8 lon=double(ncread('downloadny2018.nc','longitude')); %
   longitude coordinate
9 time=ncread('downloadny2018.nc','time'); %time
10 wind=ncread('downloadny2018.nc','wind'); %wind
11 pp1d=ncread('downloadny2018.nc','pp1d'); %peak wave
   period
12 swh=ncread('downloadny2018.nc','swh'); %significant wave
   height
13
14 LAT=[];
15 for i=1:length(lon)
16     LAT=[LAT; lat];
17 end
18
19 LON=[];
20 for j=1:length(lon)
21     for i=1:length(lat)
22         LON=[LON; lon(j)];
23     end
24 end
25
26 %% wind data
27 VD=[];
28 for i=1:length(wind(:,1,1))
29     VD=[VD; wind(i,:,1)'];
30 end
31
32 %plot wind data
33 figure('Name','Wind data 2018','NumberTitle','off')
34 map1=worldmap([18 50],[-160 -100]);
```

```
35 geoshow('landareas.shp', 'FaceColor', [0.0 0.5 0.5])
36 scatterm(LAT,LON,10,VD);
37 colormap(map1,jet)
38
39 %% wave data
40 WD=[];
41 for i=1:length(swh(:,1,1))
42     WD=[WD; swh(i,:,1)'];
43 end
44
45 %plot wave data
46 figure('Name','Wave data 2018','NumberTitle','off')
47 map3=worldmap([18 50],[-160 -100]);
48 geoshow('landareas.shp', 'FaceColor', [0.0 0.5 0.5])
49 scatterm(LAT,LON,10,WD);
50 colormap(map3,jet)
```

A.2 foil_thrust.m

```

1  %Written by Paal Furset Lader with input from Marlene
    King
2
3  function thrust=foil_thrust(k,c_xp)
4
5  % Read cd and cl
6  COEFF = read_coeff;
7
8  % Foil description
9  FOIL.chord = 1; %[m]
10 FOIL.span = 2; %[m]
11 FOIL.k = k; %[Nm/deg]
12 FOIL.xp = c_xp * FOIL.chord/2; %[m] Length from the
    center of the chord.
13
14 % Wave parameters
15 WAVE.period=3.9872; %[s]
16 WAVE.steepness=1/10; %[-]
17 WAVE.length=WAVE.period^2*9.81/(2*pi);
18 WAVE.height=0.8586; %WAVE.length*WAVE.steepness;
19 WAVE.omega=2*pi/WAVE.period;
20 WAVE.k=2*pi/WAVE.length;
21
22 T=[0:WAVE.period/100:WAVE.period];
23 U=WAVE.omega*WAVE.height/2*cos(WAVE.omega*T);
24 U2=-WAVE.omega^2*WAVE.height/2*sin(WAVE.omega*T);
25
26
27 % "Time" loop
28 for c=1:length(U)
29     Pitch(c)=find_pitch(U2(c),U(c),FOIL,COEFF);
30     [cd,cl]=find_cd_cl(COEFF,90-Pitch(c));
31     F1(c)=0.5*1025*FOIL.span*FOIL.chord*cl*U(c)^2;
32 end
33 thrust=mean(F1);
34
35
36 end
37
38 %%
39 function pitch=find_pitch(u2,u,FOIL,COEF)

```

```

40 %Iteration parameters
41 dp_max=1; %Max change in pitch from one iteration to
    the next.
42 dp_stop=0.1; %Iteration break limit
43 i_max=100; %Max number of iterations
44
45 %Initial pitch and dp
46 Pitch(1)=0; dp=90; i=1;
47
48 while and(dp>dp_stop,i<i_max)
49
50     %Angle of attack
51     alpha=90-Pitch(i);
52     [cd,cl]=find_cd_cl(COEF,alpha);
53
54     %Drag and added mass
55     Fd=0.5*1025*FOIL.span*FOIL.chord*cd*u^2; %Drag force
56     Addedmass=1025*pi*((FOIL.chord*sind(alpha)/2)^2)*
    FOIL.span*u2;
57
58     %Hydro moment
59     M=Addedmass*FOIL.xp*sind(alpha)+Fd*FOIL.xp*sind(
    alpha); %[Nm] Moment from drag force around piv point
60
61     new_pitch=M/FOIL.k; %[deg]
62
63     if abs(new_pitch-Pitch(i))>dp_max
64         Pitch(i+1)=Pitch(i)+sign(new_pitch-Pitch(i))*
    dp_max;
65     else
66         Pitch(i+1)=new_pitch;
67     end
68
69     dp=abs(Pitch(i+1)-Pitch(i));
70     i=i+1;
71 end
72
73 pitch=mean(Pitch(end-1:end));
74 end
75
76 %%
77 function [cd,cl]=find_cd_cl(COEFF,alpha)
78 %Linear interpolation

```

```
79 if alpha >= 90
80     cd=COEFF.Cd(end); cl=COEFF.Cl(end);
81 else
82     i_int=max(find(COEFF.Alpha < alpha));
83     cd=COEFF.Cd(i_int)+...
84         (COEFF.Cd(i_int+1)-COEFF.Cd(i_int))/(COEFF.Alpha
85         (i_int+1)-COEFF.Alpha(i_int))*...
86         (alpha-COEFF.Alpha(i_int));
87     cl=COEFF.Cl(i_int)+...
88         (COEFF.Cl(i_int+1)-COEFF.Cl(i_int))/(COEFF.Alpha
89         (i_int+1)-COEFF.Alpha(i_int))*...
90         (alpha-COEFF.Alpha(i_int));
91 end
92 end
93 %%
94 function COEFF = read_coeff
95 m = readtable('Coefficients.csv');
96 table = table2array(m(1:91,5:7));
97 COEFF.Alpha = table(1:91,1);
98 COEFF.Cd = table(1:91,2);
99 COEFF.Cl = table(1:91,3);
100 end
```

A.3 spring_pivot_plot.m

```
1 %Written by Paal Furset Lader with input from Marlene
   King
2
3 clear
4
5 K=[5 10 20 30 40 50 100 500 1000 5000 10000 50000 100000
   500000 1000000];
6 C=[0.1:0.1:0.9];
7
8 for c_K=1:length(K)
9     for c_C=1:length(C)
10         thrust(c_K,c_C)=foil_thrust(K(c_K),C(c_C));
11     end
12 end
13
14 fig10 = figure;
15 surf(C,K,thrust)
16 set(gca,'YScale','log')
17 xlabel('Pivot point, x_p [m]')
18 ylabel('Spring stiffness, k_s [Nm/deg]')
19 zlabel('Thrust, T [N]')
20 v = [0.5 0.5 0.5];
21 [caz,cel] = view(v);
22 print(fig10,'CKT','-depsc')
```


A.4 total_thrust.m

```

1 clear all;
2 clc;
3 close all;
4
5 %% Values
6 g = 9.81; %m/s^2
7 %Tp = 8.0727;
8 Tp = 3.9872; %s
9 H_s = 0.8586; %m
10 zeta = H_s/2; %m
11 z_1 = 0; %m
12 rho = 1025; %kg/m^3
13
14 lambda = (g/(2*pi))*Tp^2; %m
15 k = 2*pi/lambda; %1/m
16 c_w = sqrt(g/k); %m/s
17 omega = 2*pi/Tp; %1/s
18
19 %foil characteristics
20 c = 1; %m
21 b = 2; %m
22 S = b*c; %m^2
23 xf = c/4; %force center
24 xp = c/5; %pivot point
25 xa = c/2; %added mass center
26
27
28 % particle velocity
29 U = c_w*k^2*zeta^2*exp(2*k*z_1); %m/s
30
31 %% Steps
32
33 tstep = 0:Tp/100:Tp;
34 t_step = Tp/(length(tstep)-1);
35
36
37 %% Lift coeff data
38 %read NACA 0012 data
39 m = readtable('experimental.csv');
40 xltable = table2array(m(1:91,1:3));
41 xlangle = xltable(1:91,1);

```

```

42 %xlcl = xltable(1:91,2);
43 %xlcd = xltable(1:91,3);
44
45 %flat plate coefficients
46 cn1 = [];
47 xlcd = [];
48 xlcl = [];
49 for i = 1:91
50 cn = (2*pi*sind(i-1))/(4+pi*sind(i-1));
51 cn1 = [cn1 cn];
52 cd = cn*sind(i);
53 xlcd = [xlcd cd];
54 cl = cn*cosd(i);
55 xlcl = [xlcl cl];
56
57 end
58
59
60 for i = 1:length(tstep)
61     t(i) = t_step*(i-1); %s
62
63     %wave amplitude/heave motion
64     h1(i) = zeta*sin(omega*t(i)); %m
65     if abs(h1(i)) <= 10^(-10)
66         h1(i) = 0;
67     end
68
69     %heave velocity and acceleration
70     h2(i) = omega*zeta*cos(omega*t(i));
71     if abs(h2(i)) <= 10^(-10)
72         h2(i) = 0;
73     end
74     h3(i) = -(omega^2)*zeta*sin(omega*t(i));
75     if abs(h3(i)) <= 10^(-10)
76         h3(i) = 0;
77     end
78
79     %inflow velocity
80     V(i) = sqrt(h2(i)^2 + U^2);
81     if h2(i) > 0
82         V(i) = -V(i);
83     end
84     phi(i) = atand(h2(i)/U);

```

```

85
86
87     for j = 1:round(abs(phi(1)))
88         alpha(j) = xangle(j);
89         counter(j) = find(xangle == abs(
alpha(j)));
90
91         %Lift and drag
92         Cl(j) = xlcl(counter(j));
93         Cd(j) = xlcd(counter(j));
94         L(j,i) = 0.5*rho*(h2(i)^2)*S*Cl(j);
95         D(j,i) = 0.5*rho*(h2(i)^2)*S*Cd(j);
96         if h2(i) > 0
97             D(j) = -D(j);
98         end
99
100        %Pitch angle
101        if phi(i) < 0
102            theta(j,i) = -(abs(phi(i)) -
alpha(j));
103        elseif phi(i) > 0
104            theta(j,i) = phi(i) - alpha(j);
105        elseif phi(i) == 0
106            theta(j,i) = 0;
107        end
108
109        %Added mass
110        c_proj(j,i) = c*cosd(theta(j,i));
111        a_proj(j,i) = c_proj(j,i)/2;
112        m_a(j,i) = rho*pi*(a_proj(j,i)^2)*b;
113        F_a(j,i) = m_a(j,i)*h3(i);
114
115        %Hydrodynamic moment
116        M_hydro(j,i) = F_a(j,i)*(xa-xp)*cosd
(theta(j)) + ...
117        D(j,i)*sind(phi(i))*(xf-xp)*cosd
(theta(j))+ ...
118        L(j,i)*cosd(phi(i))*(xf-xp)*cosd
(theta(j));
119
120        k_s(j,i) = round(abs(M_hydro(j,i)/(
121        theta(j)))));

```

```

122         end
123
124         number = find(k_s(:,i)> 5 & k_s(:,i) <
125         10);
126         if isempty(number)
127             disp('not a feasible spring
128             stiffness')
129         elseif length(number) > 1
130             length_number = length(number);
131         end
132         for h = 1:length(number)
133             number_ = number(h);
134             theta_(h) = theta(number_,i);
135             alpha_(h) = alpha(number_);
136             L_(h) = L(number_,i);
137         end
138
139         %Maximum lift and thrust
140         L_max(i) = max(L_);
141         number_1 = find(L_ == L_max(i));
142         alpha_1(i) = alpha_(number_1);
143         theta_1(i) = theta_(number_1);
144         T_1(i) = L_max(i)*abs(sind(phi(i)));
145
146
147     end
148
149
150
151     %% Thrust
152
153     T = sum(T_1,'all')/length(T_1)
154
155     %% Plot
156
157     %Lift force
158     fig1 = figure;
159     plot(t,h1)
160     ylabel('Heave motion [m]')
161     xlabel('Time, t [s]')
162     hold on

```

```
163 yyaxis right
164 plot(t,L_max)
165 ylabel('Lift force, L [N]')
166 print(fig1,'liftforce','-depsc')
167 legend({'Lift force, L','Heave motion'},'Location','
        southwest')
168
169 %Pitch angle
170 fig2 = figure;
171 plot(t,h1)
172 ylabel('Heave motion [m] ')
173 xlabel('Time, t [s]')
174 hold on
175 yyaxis right
176 plot(t,theta_1)
177 ylabel('Pitch angle, \theta(t) [deg] ')
178 print(fig2,'theta_angles','-depsc')
179 legend({'Pitch angle, \theta','Heave motion'},'Location'
        , 'southwest')
```

B Drag and lift coefficients

B.1 Drag and lift coefficients for NACA 0012 at $R_N = 80,000$ from experiments

| | 80000.0 | NACA 0012 SECTION DATA, EPPLER MODEL, CL, CD, DEC78 | |
|---|---------|---|-------|
| 0 | 0.0000 | 0.0000 | .0133 |
| 0 | 1.0000 | .1100 | .0134 |
| 0 | 2.0000 | .2200 | .0138 |
| 0 | 3.0000 | .3300 | .0145 |
| 0 | 4.0000 | .4400 | .0155 |
| 0 | 5.0000 | .5500 | .0170 |
| 0 | 6.0000 | .6384 | .0189 |
| 0 | 7.0000 | .7227 | .0204 |
| 0 | 8.0000 | .6930 | .0222 |
| 0 | 9.0000 | -.0010 | .0600 |
| 0 | 10.0000 | .0413 | .0600 |
| 0 | 11.0000 | .0911 | .1170 |
| 0 | 12.0000 | .1430 | .1340 |
| 0 | 13.0000 | .1966 | .1520 |
| 0 | 14.0000 | .2504 | .1710 |
| 0 | 15.0000 | .3043 | .1900 |
| 0 | 16.0000 | .3582 | .2100 |

Figure 1: α , C_L and C_D for a NACA 0012 profile with $R_N = 80,000$ (Sheldahl & Klimas, 1981).

| | | | |
|---|----------|--------|--------|
| 0 | 17.0000 | .4139 | .2310 |
| 0 | 18.0000 | .4689 | .2520 |
| 0 | 19.0000 | .5232 | .2740 |
| 0 | 20.0000 | .5770 | .2970 |
| 0 | 21.0000 | .6305 | .3200 |
| 0 | 22.0000 | .6839 | .3440 |
| 0 | 23.0000 | .7373 | .3690 |
| 0 | 24.0000 | .7902 | .3940 |
| 0 | 25.0000 | .8432 | .4200 |
| 0 | 26.0000 | .8963 | .4460 |
| 0 | 27.0000 | .9496 | .4730 |
| 0 | 30.0000 | .9150 | .5700 |
| 0 | 35.0000 | 1.0200 | .7450 |
| 0 | 40.0000 | 1.0750 | .9200 |
| 0 | 45.0000 | 1.0850 | 1.0750 |
| 0 | 50.0000 | 1.0400 | 1.2150 |
| 0 | 55.0000 | .9650 | 1.3450 |
| 0 | 60.0000 | .8750 | 1.4700 |
| 0 | 65.0000 | .7650 | 1.5750 |
| 0 | 70.0000 | .6500 | 1.6650 |
| 0 | 75.0000 | .5150 | 1.7350 |
| 0 | 80.0000 | .3700 | 1.7800 |
| 0 | 85.0000 | .2200 | 1.8000 |
| 0 | 90.0000 | .0700 | 1.8000 |
| 0 | 95.0000 | -.0700 | 1.7800 |
| 0 | 100.0000 | -.2200 | 1.7500 |
| 0 | 105.0000 | -.3700 | 1.7000 |
| 0 | 110.0000 | -.5100 | 1.6350 |
| 0 | 115.0000 | -.6250 | 1.5550 |
| 0 | 120.0000 | -.7350 | 1.4650 |
| 0 | 125.0000 | -.8400 | 1.3500 |
| 0 | 130.0000 | -.9100 | 1.2250 |
| 0 | 135.0000 | -.9450 | 1.0850 |
| 0 | 140.0000 | -.9450 | .9250 |
| 0 | 145.0000 | -.9100 | .7550 |
| 0 | 150.0000 | -.8500 | .5750 |
| 0 | 155.0000 | -.7400 | .4200 |
| 0 | 160.0000 | -.6600 | .3200 |
| 0 | 165.0000 | -.6750 | .2300 |
| 0 | 170.0000 | -.8500 | .1400 |
| 0 | 175.0000 | -.6900 | .0550 |
| 1 | 180.0000 | 0.0000 | .0250 |

Figure 2: α , C_L and C_D for a NACA 0012 profile with $R_N = 80,000$ (Sheldahl & Klimas, 1981).

